INEEL/EXT-01-00894

Transport Models for Radioactive Carbon Dioxide at RWMC

L. C. Hull
F. A. Hohorst

December 2001

Idaho National Engineering and Environmental Laboratory
Bechtel BWXT Idaho, LLC

INEEL/EXT-01-00894

Transport Models for Radioactive Carbon Dioxide at RWMC

Larry C. Hull
Fred A. Hohorst

December 2001

Idaho National Engineering and Environmental Laboratory
Idaho Falls, Idaho 83415

Prepared for the
U.S. Department of Energy

Under DOE Idaho Operations Office
Contract DE-AC07-99ID13727

ABSTRACT

Radioactive carbon dioxide (formed by oxidation of carbon-14) is a highly mobile, radioactive contaminant released from solid wastes buried at the Subsurface Disposal Area (SDA) at the Radioactive Waste Management Complex (RWMC) at the Idaho National Engineering and Environmental Laboratory (INEEL). Radioactive CO_2 is chemically active in the environment, volatile, water soluble, and subject to adsorption on solids. For this reason, its fate must be understood and controlled to meet radiological requirements (protection of the atmosphere, aquifer, vadose zones, plants and animals). In the present work, the migration of carbon-14 as dissolved bicarbonate was studied using miscible displacement experiments in water-saturated columns containing sediments from RWMC. Dissolved carbon-14 was retarded relative to the movement of water by a factor of about 3.6, which translates to a partition coefficient (K_d) of 0.8 ml/g. Two different adsorption sites were identified, with one site possibly having a nonlinear adsorption isotherm. A conservative tracer gas, sulfur hexafluoride, was used to measure the tortuosity of sedimentary material for gaseous diffusion. The tortuosity of the RWMC sediment (Spreading Area B sediment) was determined to be 3.2, which is slightly greater than predicted by the commonly used Millington-Quirk equation. In terms of affecting the migration of carbon-14 to the aquifer, the relative importance of the parameters studied is: (1) natural moisture content of the sediments, (2) sediment tortuosity to gas-phase diffusion, and (3) adsorption onto solid phases.

CONTENTS

ABSTRACT iii

ACRONYMS ix

1. INTRODUCTION 1

2. BACKGROUND 2

2.1 Adsorption 2

2.2 Transport 3

2.3 Diffusion 5

3. EXPERIMENTAL PROGRAM 8

3.1 Sediment Properties 8

3.2 Miscible Displacement 8

3.2.1 Experimental Materials 8
3.2.2 Experimental Conditions 10
3.2.3 Data Reduction 11

3.3 Transport in Water 12

3.4 Diffusion 20

3.4.1 Experimental Materials 20
3.4.2 Experimental Conditions 21
3.4.3 Data Reduction 21

3.5 Diffusion in the Gas Phase 22

4. RESULTS AND DISCUSSION 27

5. CONCLUSIONS 31

6. REFERENCES 32

Appendix A—Evaporation of Water from Sample Tubes 39

Appendix B—Losses of Carbon-14 during Sample Collection 43

Appendix C—Description of the EFD1D Code for Estimation of Mass Flux from Gas Diffusion and Aqueous Advection in One-Dimension 51

FIGURES

1. The effective gas phase diffusion coefficient decreases as the pores in a porous medium fill with water, decreasing the air-filled porosity. Total porosity is 0.5. 6

2. Coefficient of longitudinal dispersion as a function of velocity for column experiments..... 11

3. Distribution of carbon-14 in column sediments after second breakthrough test. 13

4. Breakthrough curve of tritium (symbols) for Test A and best-fit breakthrough curve determined using CXTFIT (line). 14

5. Breakthrough curve of tritium (symbols) for Test B and the best-fit breakthrough curve determined using CXTFIT (line). 14

6. Plot of carbon-14 breakthrough concentrations (symbols) for Test B and a best-fit model using CXTFIT (line) assuming equilibrium, reversible adsorption of carbon-14 and physical transport properties determined from tritium transport. 15

7. Plot of carbon-14 breakthrough concentrations for Test A (symbols) and a best-fit model (line) using a two-site kinetic adsorption model. Advective velocity and dispersion fixed by tritium. 16

8. Plot of carbon-14 breakthrough data (symbols) from Test B and a best fit curve using CXTFIT (line) using a two site, kinetic adsorption model. Advective velocity and dispersion determined from the tritium breakthrough curve..... 16

9. Plot of a Freundlich isotherm (solid line) fit to the carbon-14 breakthrough curve (symbols) for Test B compared to the CXTFIT result for the two-site conceptual model. 19

10. Plot of a Freundlich isotherm (solid line) fit to the carbon-14 breakthrough curve (symbols) for Test A compared to the CXTFIT result for the two-site conceptual model..... 19

11. Experimental apparatus for measuring diffusion coefficients in sediments. 21

12. Source chamber sulfur hexafluoride concentrations for all diffusion experiments. 24

13. Plot of sulfur hexafluoride concentration in the source reservoir as a function of time for the test conducted June 29 and the fit of a linear regression to the data..... 24

14. Fit of diffusion model wit D_m = 2.08 cm^2/min to sulfur hexafluoride test data collected June 29.. 25

15. Change in effective diffusion coefficient for soil gas as a function of air-filled porosity. 26

16. Plot of carbon dioxide concentration in the source reservoir as a function of time for the test conducted June 29, and one possible fit of a linear regression to a portion of the data between 500 and 2,700 minutes. 26

A-1. Water lost from sample collection tubes by evaporation measured by weight loss. 38

B-1. Schematic diagram of the flow-through chamber used to measure the loss of carbon-14 from fraction collector tubes. 43

B-2. Schematic diagram of the experimental apparatus and support equipment used to measure the loss of carbon-14 from fraction collector tubes. 44

C-1. Conceptual model of the EFD1D code for vapor diffusion and aqueous phase advective transport. 50

TABLES

1. Representative exponents from the literature for the dependence of gas diffusion in pores as a function of air-filled porosity and total porosity for Equation 9. 6

2. Composition of synthetic soil water used in column experiments. 9

3. Experimental conditions for the miscible displacement column tests. 10

4. Conditions and parameters for carbon-14 miscible displacement tests. 12

5. Freundlich isotherm parameters estimated by inverse modeling of the carbon-14 breakthrough data from the laboratory columns. 18

6. Effective gas-phase diffusion coefficient of carbon dioxide in the SDA calculated for different soil-moisture content and different relations between moisture and tortuosity, with total porosity equal to 0.45 and a free air diffusion coefficient of 16,000 cm^2/day 28

7. Calculated apparent gas-phase diffusion coefficients incorporating both tortuosity effects and the capacity factor, which accounts for partitioning of carbon dioxide from the gas phase to vadose zone water and sediments. 28

8. Vadose zone properties at the subsurface disposal area for dry and wet conditions (Bishop 1998). 29

9. Percent of initial carbon dioxide in the source that is released to the atmosphere by diffusion over a period of seven years, as a function of transport parameters used in the simulation. 29

B-1. Room temperature during volatilization experiments. 45

B-2. Net carbon-14 activity released from the fraction collector tube as a function of time 46

B-3. Fraction of carbon-14 retained in the fraction collector tube as a function of time 47

C-1. Input file format for the EFD1D code. Default file name is EFD1D.PAR. Comments can be added by placing a $ in the first column of a line. 55

ACRONYMS

INEEL	Idaho National Engineering and Environmental Laboratory
RWMC	Radioactive Waste Management Complex
SDA	Subsurface Disposal Area

Transport Models for Radioactive Carbon Dioxide at RWMC

1. INTRODUCTION

The Subsurface Disposal Area (SDA) within the Radioactive Waste Management Complex (RWMC) at the Idaho National Engineering and Environmental Laboratory (INEEL) is a disposal site for solid radioactive waste. Since the 1950s, waste has been buried at the 40-hectare site in soil vaults, pits, and trenches, and covered with a minimum of one meter of fine-grained sediment excavated from a nearby playa known as Spreading Area B. Before 1970, SDA disposals included low-level and transuranic radioactive waste. Since 1970, only low-level radioactive waste has been buried at the SDA.

A radiological performance assessment, as required by U. S. Department of Energy Order 425.1, was performed for the SDA (Maheras et al. 1994). Since the performance assessment was completed, additional information has been found indicating that the amount of carbon-14 in the waste may be greater than the amount used in the performance assessment. Subsequent risk analysis based on the increased inventory (McCarthy et al.2000; Case et al.2000) raises the possibility that species containing carbon-14 could migrate to the Snake River Plain Aquifer underlying the SDA at concentrations that could expose a future resident to doses of radioactivity that exceed U. S. Department of Energy protection criteria.

The radiological performance assessment and subsequent analysis considered chemicals containing carbon-14 to migrate only in the dissolved phase with groundwater being the only migration pathway. Carbon-14 released from buried waste at the SDA is primarily in the form of carbon dioxide (Ritter, McElroy, and Bhatt 1997). Carbon dioxide is a soluble gas and partitions between the water and gas phases. It migrates by diffusion in the gas phase as well as by downward advection of soil water. Some of the carbon dioxide in the soil diffuses upward to the atmosphere (Solomon and Cerling 1987; Simunek and Suarez 1993; Suarez and Simunek 1993). This would decrease the carbon-14 inventory available for downward migration to the aquifer and affect the dose via the groundwater pathway. Furthermore, the radiological performance assessment did not consider partitioning of species containing carbon-14 between the dissolved phase and the solid phases in the vadose zone. Partitioning between dissolved and solid phases retards carbon-14 migration to the aquifer. This investigation was conducted to obtain data to more reliably predict the migration of carbon-14 in radioactive carbon dioxide and its derivatives, from sources buried at the SDA.

2. BACKGROUND

Radioactive carbon-14 in buried waste at the SDA was primarily produced in nuclear reactors by neutron bombardment of carbon-13 and nitrogen-14 contained in metal reactor components. Metal components removed from reactors and disposed of as buried waste begin to corrode in the subsurface. As the metal corrodes, carbon-14 in the metal is oxidized to radioactive carbon dioxide. Beryllium reflector blocks are particularly susceptible to corrosion and are a principle source of radioactive carbon dioxide in the SDA (Ritter, McElroy, and Bhatt 1997). Therefore, knowledge of the movement of carbon-14 in the vadose zone requires knowledge of the properties and movement of carbon dioxide and associated aqueous carbonate species.

Carbon dioxide in the vadose zone partitions among solid, liquid, and gas phases. Carbon dioxide from the gas phase dissolves in pore water to form various carbonate species [CO_2(aq), HCO_3^-, CO_3^{-2}]. Because CO_2(aq) dissociates to bicarbonate and carbonate species as a function of pH, the partitioning between gas phase and aqueous phase is a function of the pH of the vadose zone pore water. Dissolved carbonate adsorbs onto mineral surfaces. The transport of carbon dioxide in the vadose zone, therefore, depends on partitioning among three phases. Because of complex interactions between multiple phases, two end member systems were identified for this investigation. The two systems investigated were: (1) a saturated flow condition where a gas phase is not present, and (2) an unsaturated system where all transport occurs by diffusion in the gas phase.

2.1 Adsorption

Partitioning of dissolved carbon dioxide from the aqueous phase to SDA sedimentary materials (solid phase) may retard carbon-14 migration. Relatively few measurements have been made for carbon-14 adsorption on natural materials. Most studies have been conducted on calcite or mixtures of calcite and sands (Martin 1996; Garnier 1985; Mozeto, Fritz, and Reardon 1984) and ferric oxyhydroxides (Zachara et al. 1987; van Geen et al. 1994). While anion adsorption on ferric oxyhydroxides has shown to be important, the total volume of work on oxides is limited. Studies conducted on natural sediments (Allard, Torstenfelt, and Andersson 1981; Striegl and Armstrong 1990; Martin 1996; Dicke and Hohorst 1997) are even more limited. Batch adsorption experiments on sediments from the SDA were conducted by Dicke and Hohorst (1997) for carbon-14 adsorption.

Partitioning between aqueous and solid phases is often described by a linear distribution coefficient (K_d). The distribution coefficient is calculated from the ratio of the carbon-14 concentration on the solid phase to the concentration in solution:

$$K_d = \frac{C_s}{C_l} \tag{1}$$

where

C_s = concentration on the solid phase (pCi/g)

C_l = concentration in the liquid phase (pCi/ml)

K_d = linear, reversible distribution coefficient (ml/g).

Distribution coefficients depend on the contact time in experiments and on the solid phase used. In batch adsorption experiments with a variety of natural sedimentary materials, Allard, Torstenfelt, and Anderson

(1981) found that K_d values stabilize in the range of 1.1 to 3.0 ml/g after about one to five weeks of contact time. Calcite was different in this regard, showing increased adsorption over time with very high distribution coefficients (83 ml/g) obtained after six months. Other batch adsorption experiments with sedimentary materials have found K_d values for carbon-14 to be generally low. Martin (1996) measured K_d values in the range of 3.5 to 4.6 ml/g for Hanford sediments and Dicke and Hohorst (1997) measured K_d values in the range of 0.1 to 2.0 ml/g for sediments collected at the SDA.

A species that reversibly adsorbs to solids spends part of its time moving with the water phase, and part of its time attached to solid surfaces. Therefore, the velocity at which an adsorbing species moves through the vadose zone is slower than the velocity at which the water moves. If adsorption is described by a linear partition coefficient (Equation 1), the retardation factor is given by:

$$R = 1 + \frac{\rho_b}{\theta_w} K_d \tag{2}$$

where

R = retardation factor (dimensionless)

ρ_b = dry bulk density (g/cm^3)

θ_w = volumetric water content (cm^3/cm^3).

For typical INEEL sedimentary materials, the bulk density ranges from 1.3 to 1.8 g/cm^3 and the porosity ranges from 0.3 to 0.5 cm^3/cm^3 (Barraclough et al.1976). The ratio of sediment bulk density to porosity, therefore, is generally in the range of 3 to 5. For a K_d of 1 ml/g, then, the retardation factor is in the range of 4 to 6.

2.2 Transport

Adsorption onto solid phases is only one of a number of processes that will govern the transport of a solute through a porous medium. The theory of transport is well developed and has been documented in the literature (van Genuchten and Wierenga 1976; Nkedi-Kizza et al. 1984; van Genuchten and Wagenet 1989; Toride, Leij, and van Genuchten 1995). A comprehensive treatment of transport includes advection with the moving fluid, dispersion from mixing as water moves at different velocities along different flow paths, equilibrium adsorption onto solid phases, kinetic adsorption onto solid phases, diffusion from actively moving water to non-mobile water, and sources or sinks for the solute. Most treatments of radionuclide migration consider advection, dispersion, radioactive decay, and reversible linear sorption.

In some soils, soil water can be divided into mobile and immobile fractions. For this type of soil, a two-region non-equilibrium model of transport is used. In situations where non-equilibrium adsorption is an important process, a two-site non-equilibrium model of transport is used. Mathematically, the two models have been shown to be the same (Nkedi-Kizza et al. 1984). To differentiate between physical and chemical non-equilibrium processes, multiple tracers must be used with different properties.

A computer program, CXTFIT, has been developed incorporating non-linear least squares curve fitting algorithms to determine transport parameters using breakthrough data from laboratory columns (Toride, Leij, and van Genuchten 1995). For steady-state flow in a homogeneous column of sediment, transport of a linearly adsorbing solute with two adsorption sites (equilibrium and kinetic) and radioactive decay is given by:

$$\left(1+\frac{f\rho_b K_d}{\theta_w}\right)\frac{\partial C_l}{\partial t} = D_l\frac{\partial^2 C_l}{\partial x^2} - v\frac{\partial C_l}{\partial x} - \frac{k\rho_b}{\theta_w}\left[(1-f)K_d C_l - C_k\right] - \lambda C_l - \frac{f\rho_b K_d \lambda C_l}{\theta_w} \quad (3)$$

$$\frac{\partial C_k}{\partial t} = k\left[(1-f)K_d C_l - C_k\right] - \lambda C_k \quad (4)$$

where

C_k = concentration on the kinetic adsorption sites (pCi/g)

D_l = coefficient of longitudinal hydrodynamic dispersion (cm^2/min)

v = advection velocity (cm/min)

k = first-order kinetic rate coefficient for adsorption (min^{-1})

λ = radioactive decay coefficient (min^{-1})

f = fraction of exchange sites that are equilibrium sites

x = distance coordinate (cm)

t = time (min).

The fraction of adsorption sites that are equilibrium sites, and a dimensionless rate term can be developed to describe the reaction rate onto the kinetic adsorption sites:

$$\beta = \frac{\theta_w + f\rho_b K_d}{\theta_w + \rho_b K_d} \quad (5)$$

$$\omega = \frac{k(1-\beta)RL}{v} \quad (6)$$

where

l = Length of column (cm).

When fitting transport equations to data, CXTFIT estimates the dimensionless parameters. For the laboratory experiments conducted in this investigation, the duration of the experiments (a few days) is short compared to the half-life of tritium (12.3 years) and carbon-14 (5,715 years), and so the radioactive decay terms are negligible.

2.3 Diffusion

Numerous studies have been conducted to determine the relation between diffusion of gases in porous media and the air-filled porosity of the medium. Many relations between porosity and gas-phase diffusion have been suggested and tested (Millington 1959; Currie 1960a; Currie 1960b; Weeks, Earp, and Thompson 1982; Sallam, Jury, and Letey 1984; Kreamer, Weeks, and Thompson 1988; Lerman 1988). Particle shape and particle size distribution affect gas diffusion and how diffusion changes with moisture content. The diffusion coefficient in a porous medium is lower than the diffusion coefficient in air by an amount described by the tortuosity factor (Grathwohl 1998).

$$D_{eff} = \frac{D_{air}}{\tau_g} \tag{7}$$

where

D_{eff} = effective gas phase diffusion coefficient in the soil gas (cm^2/min)

D_{air} = gas phase diffusion coefficient in air (cm^2/min)

τ_g = tortuosity factor (dimensionless).

A number of relations have been proposed relating the tortuosity factor to air-filled and total porosity. Many of these relations take the general form of:

$$\tau_g = \frac{\theta_t^n}{\theta_g^m} \tag{8}$$

θ_t = total porosity (cm^3/cm^3)

m = exponential dependence of diffusion on air-filled porosity

n = exponential dependence of diffusion on total porosity.

Substituting Equation 8 back into Equation 7 gives a functional dependence of effective gas-phase diffusion in a partially saturated porous media on porosity:

$$D_{eff} = D_{air} \frac{\theta_g^m}{\theta_t^n} \tag{9}$$

Typical values for *m* and *n* are shown in Table 1 and the relations are illustrated in Figure 1.

Table 1. Representative exponents from the literature for the dependence of gas diffusion in pores as a function of air-filled porosity and total porosity for Equation 9.

Reference	m	n	m-n
Sallam et al. (1984)	2.10	2	0.10
Millington (1959)	2.33	2	0.33
Currie (1970)	4.0	3.5	0.50

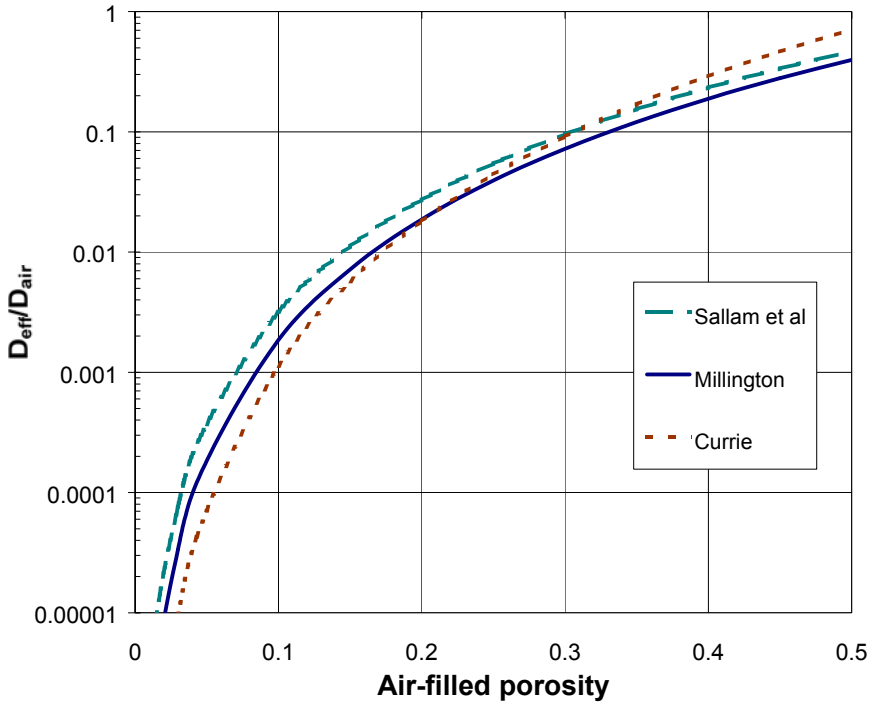

Figure 1. The effective gas phase diffusion coefficient decreases as the pores in a porous medium fill with water, decreasing the air-filled porosity. Total porosity is 0.5.

As the soil dries, the pores become filled with air and θ_g approaches θ_t. Under dry conditions, simplifying Equation 9 gives:

$$D_{eff} = D_{air}\theta_t^{m-n} \tag{10}$$

In studies of dry, granular materials, Currie (1960b) found that the difference between *m* and *n* ranged from 0.4 for spheres of uniform size to a little over 2 for clays to as much as 10 for powdered materials. The difference between *m* and *n* for the empirical coefficients listed in Table 1 tend to be near the low end of this range suggesting that these relations were developed for coarser soil materials.

In addition to the physical effects of pore tortuosity on diffusion, a gas can partition to the pore water, partition to solid phases in the soil, and react in the pore water. The migration of a reactive gas moving through a variably saturated media has been investigated (Weeks, Earp and Thompson 1982; Kreamer, Weeks, and Thompson 1988; Gierke, Hutzler, and Crittenden 1990). Partitioning between the gas phase and the aqueous phase and between the aqueous phase and solid phases retards the diffusion of the reactive gas. A retardation factor for diffusion of a reactive gas can be defined by (Weeks et al. 1982):

$$R = 1 + \frac{\theta_w}{\theta_g K_H} + \frac{\rho_b K_d}{\theta_g K_H} \tag{11}$$

where

K_H = Henry's Law partition coefficient (dimensionless).

R (Equation 11) is also referred to as the Capacity Factor (Grathwohl 1998) because it accounts for the capacity of the partially saturated sediment to retard the movement of a diffusing gas under transient conditions. An apparent gas phase diffusion coefficient (D_{app}) is defined by Grathwohl (1998) for a reactive gas that has a linear adsorption isotherm by combining Equations 7 and 11 and including θ_g to represent the cross-sectional area available for diffusion:

$$D_{app} = \frac{D_{eff}}{R} = \frac{\theta_g D_{air} / \tau_g}{1 + \left(\theta_w \middle/ \theta_g K_H \right) + \left(\rho_b K_d \middle/ \theta_g K_H \right)} \tag{12}$$

While the solubility of carbon dioxide in water is well documented, the solubility is not constant at a given temperature, but is a function of pH. Using data for the solubility of carbon dioxide and the dissociation of carbonate species (Harned and Scholes 1941; Harned and Davis 1943; Harned and Bonner 1945), at pH of 7.5 and temperature of 23°C, the Henry's Law coefficient will be:

$$K_H = \frac{H}{RT} = \frac{10^{1.41} 10^{-3}}{\left(1 + 10^{-6.39} \middle/ 10^{-7.5}\right) RT} = \frac{1.85 x 10^{-3}\, atm \cdot m^3 / mole}{RT} = 0.076 \tag{13}$$

where

H = carbon dioxide solubility (moles/liter)

R = ideal gas constant (atm m^3/mole°K)

T = temperature (°K).

The apparent diffusion coefficient describes the diffusion of a reactive gas diffusing through a partially saturated porous medium.

3. EXPERIMENTAL PROGRAM

The experimental program was designed to evaluate conceptual transport models of carbon dioxide and related compounds which might host carbon-14 in the SDA sediments. For this purpose, soil samples were taken from the Spreading Area B Site at RWMC and packed in laboratory columns for evaluation of mobility parameters for CO_2 and its derivatives.

3.1 Sediment Properties

Spreading Area B sediment obtained from playa lakebeds west of the SDA was used for this investigation. This sediment has been used as a cover material for the SDA and is similar to the fine-grained materials found inside the SDA. Spreading Area B sediment properties have been determined by Tullis et al. (1993) and Hull et al. (1999). This sediment contains 20% very fine sand, 60% silt, and 20% clay. The surface area is 32 m^2/g. The calcium carbonate content ranges from 2 to 20% and averages 9%, with higher concentrations occurring in layers where paleosols have developed. The pH of a saturated paste ranges from 7.7 to 8.1 with an average of 7.9. This very narrow range of pH values is indicative of a calcareous material where the pH of the saturated paste reflects saturation of the solution with calcite in equilibrium with atmospheric carbon dioxide. The organic matter content is very low, with organic carbon averaging about 0.2% with slightly higher values in the A and upper B soil horizons. The cation exchange capacity ranges from 42 to 54 meq/100 g and is dominated by calcium on the exchange sites. The clay mineralogy consists primarily of illite, smectite, and mixed-layer illite-smectite with minor amounts of kaolinite (Rightmire 1984; Rightmire and Lewis 1987; Bartholomay, Knobel, and Davis 1989). The clay minerals are primarily detrital (Bartholomay 1990).

3.2 Miscible Displacement

Miscible displacement experiments were conducted to obtain direct measurement of retardation of carbon-14 in sedimentary material similar to material at the SDA. Fitting breakthrough curves of carbon-14 from the column using transport models permits estimation of transport parameters that can be used in performance assessment models.

3.2.1 Experimental Materials

Miscible displacement experiments were conducted in a Plexiglas column 30.5 cm long and 5 cm in diameter. The column was packed with air-dried Spreading Area B sediment. Sediment was sieved through an 850 micrometer sieve to remove larger particles and organic debris. Sediment was added to the column in 2.5 cm lifts. Each lift was compacted before the next lift was added. The Plexiglas column was weighed before and after filling with sediment to obtain the mass of sediment added to the column. Bulk density was calculated as the mass of added sediment divided by the volume of the column. Air was displaced from the column with carbon dioxide prior to filling with water. Any gas bubbles trapped during the filling process, therefore, consisted of carbon dioxide, which is highly soluble in water. Extensive flushing of the column was not necessary to displace entrapped air. The column was again weighed after filling with water and the porosity of the column calculated from the weight gain upon addition of water. The bulk density of the column used for the miscible displacement experiments was 1.45 g/cm^3 with a porosity of 0.46 cm^3/cm^3.

The water used in the experiments was a synthetic soil water. Because dissolution and precipitation of calcite was of concern as a mechanism for removing carbon-14 from solution, an artificial solution was designed to be very close to saturation with respect to calcite. Water samples collected from the SDA using porous cup lysimeters were used as the basis of the synthetic soil water. Relatively low ionic

strength SDA soil waters were used as the basis of design. Table 2 shows the chemical composition of the synthetic soil water. This water is saturated with respect to calcite and has a partial pressure of carbon dioxide of $10^{-2.2}$ atm. Because of the elevated partial pressure of carbon dioxide relative to atmospheric carbon dioxide, loss of carbon dioxide from the synthetic soil water was a concern. Synthetic soil water was made up immediately before each experiment. Feed solutions were placed in intravenous solution bags with no vapor phase. As feed solution was introduced to the column, the bag collapsed preventing build-up of a vapor phase over the solution.

Table 2. Composition of synthetic soil water used in column experiments.

Chemical	Concentration (mg/L)
Ca^{+2}	63
Mg^{+2}	29
Na^{+}	96
K^{+}	3.9
HCO_3^{-}	230
Cl^{-}	53
SO_4^{-2}	220
pH	7.47
Saturation index for calcite	0.0
Saturation index for gypsum	-1.40
Partial pressure of carbon dioxide	$10^{-2.2}$ atm

Tracers used to study the transport properties of the sediment column were bromide, tritium, and sodium carbonate labeled with carbon-14. Bromide and tritium are conservative tracers and were used to quantify the physical transport properties of the sediment. Radioactively labeled sodium carbonate was added to give 3.7 to 9.1 nCi/ml of carbon-14. This translates to 2×10^{-5} to 5×10^{-5} molar radioactive carbonate out of a total dissolved carbonate concentration of 3.8×10^{-3} molar.

Solution was introduced into the column using a high-pressure liquid chromatography pump. Column pressures were on the order of 30 to 100 kPa above atmospheric pressure. Effluent from the column was tested for tracers using either a bromide-specific ion electrode or by collecting water samples from the outlet with a fraction collector. The pH of the effluent was monitored continuously with a flow-through glass combination pH electrode.

Carbon-14 and tritium were measured on samples collected from column effluent with a fraction collector. Fraction collector tubes were capped frequently, but a maximum of 16 hours could elapse between the time a tube was filled and the time the tube was capped. Evaporation from the tubes and loss of carbon-14 by volatilization between the time the tube was filled and the time the tube was capped were considered possible interferences. Evaporation from the tubes was measured to be 0.0043 mL/hr (Appendix A). Over a 16-hour period, potential loss by evaporation is calculated to be 0.3%. Sodium carbonate was added to the fraction collector vials to prevent volatilization of carbon dioxide and loss of carbon-14. Experiments conducted on loss of carbon-14 from fraction collector vials (Appendix B) showed a loss of less than 3 percent of carbon-14 from the vials under conditions similar to those of the column experiments. Carbon-14 and tritium were measured by scintillation counting.

3.2.2 Experimental Conditions

Tritium and bromide were used as conservative tracers to study the physical transport properties of the column. The average breakthrough of tritium and bromide is a measure of the advection velocity. The spread of the tritium and bromide breakthrough curves is a measure of the dispersion. Tritium and bromide can also be used to test for a physical non-equilibrium situation to determine the rate of diffusion into the immobile water fraction. Tritium and bromide data establish the physical transport environment so that the number of unknown variables can be reduced to the chemical parameters for evaluation of carbon-14 transport.

Three one-column experiments were conducted using sodium bromide, and two one-column experiments conducted with tritium to determine basic transport characteristics of the sediment column. All tests were conducted under water-saturated conditions. Table 3 shows the flow conditions of the miscible displacement experiments. Advective velocities in the experiments were kept low. In the fastest flow-rate experiment, the advective velocity was only 0.13 cm/min.

Table 3. Experimental conditions for the miscible displacement column tests.

Injection Rate (cm^3/min)	Velocity (cm/min)	Residence time (min)	Longitudinal Dispersion (cm^2/min)	Dispersivity (cm)	Tracer
0.44	4.51E-02	671	2.53E-03	5.60E-02	Tritium
0.56	5.77E-02	500	2.47E-03	4.28E-02	Bromide
0.82	8.40E-02	360	4.12E-03	4.90E-02	Bromide
1.01	1.05E-01	292	4.08E-03	3.91E-02	Tritium
1.30	1.33E-01	227	6.12E-03	4.60E-02	Bromide

The column residence times of four to eleven hours are short relative to the time for equilibrium to be attained in batch sorption experiments (on the order of one to two days [Dicke and Hohorst 1997]). Reaction rates are a function of the surface area to volume ratio (Bethke 1996). A typical batch experiment might be run with 1 g of sediment in 30 ml of solution in a centrifuge tube (ASTM 1993) for a surface area to volume ratio of:

$$\frac{1\ g\ soil \cdot 30\ m^2/g}{30\ ml} = 1\ m^2/ml \tag{14}$$

For the sediment column, the ratio is:

$$\frac{1.45\ g/cm^3 \cdot 30\ m^2/g}{0.46\ ml/cm^3} = 95\ m^2/ml \tag{15}$$

In the sediment column, reaction rates are expected to be 100 times faster than in a batch reactor. What takes 48 hours in a batch reactor might take 30 minutes in a sediment column. Even though reaction rates are faster in the column, the water travels an appreciable distance in 30 minutes. Therefore, kinetic adsorption effects are possible in the column experiments.

3.2.3 Data Reduction

Breakthrough curves from the experiments were analyzed using the computer program CXTFIT from the U. S. Salinity Laboratory (Toride, Leij, and van Genuchten 1995). Bromide and tritium breakthrough curves were used to determine the dispersive characteristics of the sediment column. These were then fixed and the carbon-14 breakthrough curves were analyzed for reactive characteristics using the determined physical characteristics. Table 3 shows the dispersive characteristics of the sediment determined from the bromide and tritium experiments. The velocity and dispersion data are plotted in Figure 2. The theoretical definition of dispersion is given by the equation:

$$D_l = \alpha v + D_{pw} \tag{16}$$

where

D_l = longitudinal dispersion coefficient (cm^2/min)

α = dispersivity coefficient (cm)

v = advective velocity (cm/min)

D_{pw} = water phase diffusion coefficient in porous media (cm^2/min).

A linear relation between dispersion and velocity is shown with a slope of 0.04 ± 0.02 cm, an intercept of 0.0004 ± 0.0019 cm^2/min and an r^2 of 0.925. From Equation 16, these results give a dispersivity coefficient of 0.04 cm and a coefficient of molecular diffusion of 4×10^{-4} cm^2/min. The diffusion coefficient, with these few points, is not significantly different than 0.0 at the 95% confidence level.

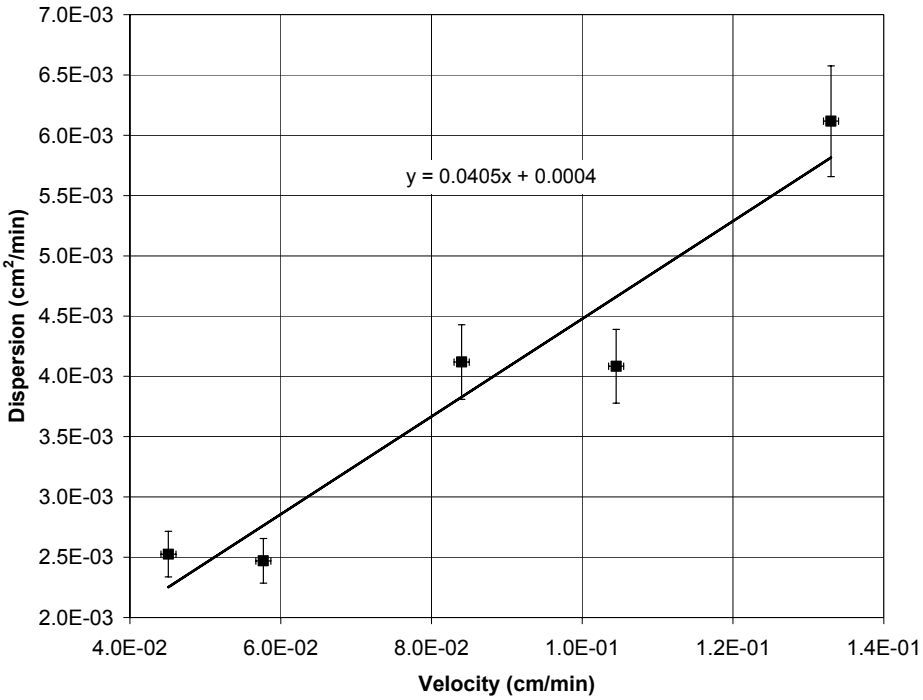

Figure 2. Coefficient of longitudinal dispersion as a function of velocity for column experiments.

3.3 Transport in Water

Two tests were conducted with carbon-14 as a reactive tracer. Test A was conducted at an injection rate of 0.44 cm^3/min with a corresponding advective velocity of 0.045 cm/min (Table 4). Test B was conducted at an injection rate of 1.01 cm^3/min with a corresponding advective velocity of 0.105 cm/min. The residence time in the column for Test A was 11.3 hours, and for Test B was 4.8 hours. For each test, approximately one-half of a pore volume of fluid containing radioactive tracer was injected into the column.

Table 4. Conditions and parameters for carbon-14 miscible displacement tests.

Injection rate (cm^3/min)	Velocity (cm/min)	Pore volumes injected	Carbon-14 concentration injected (nCi/ml)	Tritium concentration injected (nCi/ml)	Test reference name
0.44	4.51E-02	0.44	3.7[a]	3.4	Test A
1.01	1.05E-01	0.52	9.1	6.3	Test B

a. Injection concentration adjusted for mass balance.

All column experiments were conducted on the same packed sediment column. No carry-over of bromide or tritium was observed. Nonreversible sorption of carbon-14 could result in retention of carbon-14 in the column. This possibility was evaluated by analyzing the carbon-14 content of the sediment in the column at the end of the experiment. The area under the tracer breakthrough curves was integrated to determine the recovery of the tritium and carbon-14 tracers. In the first tritium breakthrough test (Test A), instrument difficulties resulted in only the latter half of the tritium peak being sampled. The estimated tritium mass balance for Test A was low, but considerable uncertainty exists in the recovery curve. The carbon-14 breakthrough curve occurred much later than the tritium breakthrough curve on Test A, and sampling equipment was working when the carbon-14 breakthrough occurred. The carbon-14 recovery calculated from Test A was only 75%, suggesting significant retention in the sediment column. This calculated under-recovery amounts to about 120 nCi of the 480 nCi of carbon-14 injected. For the second breakthrough test, Test B, tritium recovery was 100% and carbon-14 recovery was 103%.

After the completion of the experiment, the sediment column was dismantled, and samples of the sediment analyzed for carbon-14. Approximately 26 nCi of carbon-14 remained in the column at the end of the experiment (Figure 3). The total amount of carbon-14 injected in the two tests was 1000 nCi. The mass balance calculated over the two experiments indicates a net loss of carbon-14 of about 94 nCi. However, only 26 nCi, or about 3% of the total mount injected, remained in the column at the end of the experiment. Therefore, the mass balance problems with Test A cannot all be attributed to retention in the sediment column. Loss of carbon-14 from the fraction collector tubes is estimated to be less than 3% based on volatilization experiments described in Appendix B. There was some variation in measurements of carbon-14 concentration in the feed solution, which may have been due to incomplete mixing of the feed solution. The most likely explanation for the discrepancy in the mass balance is that the feed solution concentration was overestimated. Therefore, the injection concentration for Test A was adjusted to give mass balance over the two tests (Table 4).

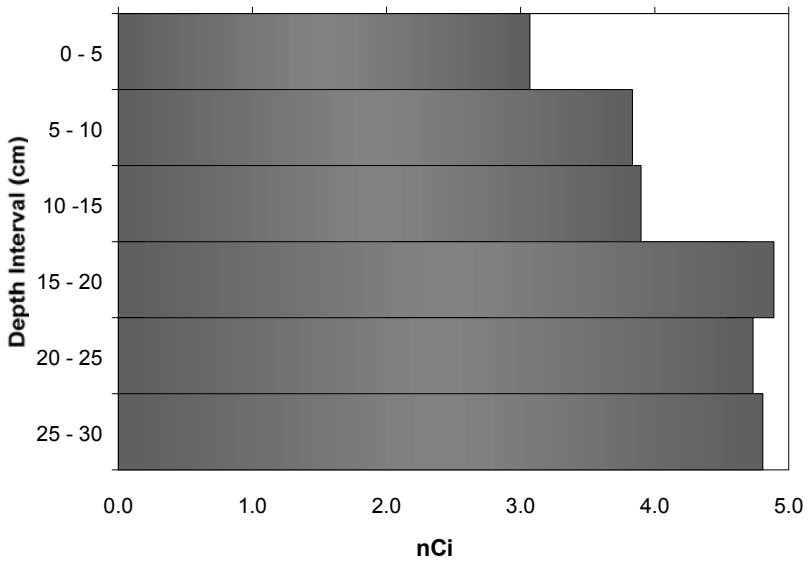

Figure 3. Distribution of carbon-14 in column sediments after second breakthrough test.

Transport of tritium in the Spreading Area B sediment column was analyzed using CXTFIT to determine transport parameters. For tritium and bromide experiments, CXTFIT was used to assess the physical processes advection, dispersion, and physical non-equilibrium (diffusion into immobile water regions). The advection velocity estimated by CXTFIT matched the velocity calculated from the injection rate and the calculated porosity. The parameters estimated by CXTFIT for physical non-equilibrium were not significant, so there is no evidence of immobile pore water in the column. Figure 4 shows a plot of the experimental tritium data and the breakthrough curve based on the parameters determined by CXTFIT for Test A, and Figure 5 shows the same information for Test B. The processes considered important for tritium are advection at the average linear velocity of the pore fluid and dispersion. The results indicate that there are no immobile water zones in the column into which tracer could diffuse. There is also no indication of adsorption of tritium onto solids.

Advection and dispersion are physical processes, and so it was assumed that advection and dispersion for carbon-14 would be the same as advection and dispersion for tritium. Any delay in the carbon-14 breakthrough or change in shape of the breakthrough curve, would be due to chemical processes, not physical processes. Figure 6 shows a plot of the observed carbon-14 breakthrough curve from the column for Test B and a line representing the best fit model based on linear, reversible one-site adsorption of carbon-14. This is the model most generally used for performance assessment. The calculations were made using CXTFIT.

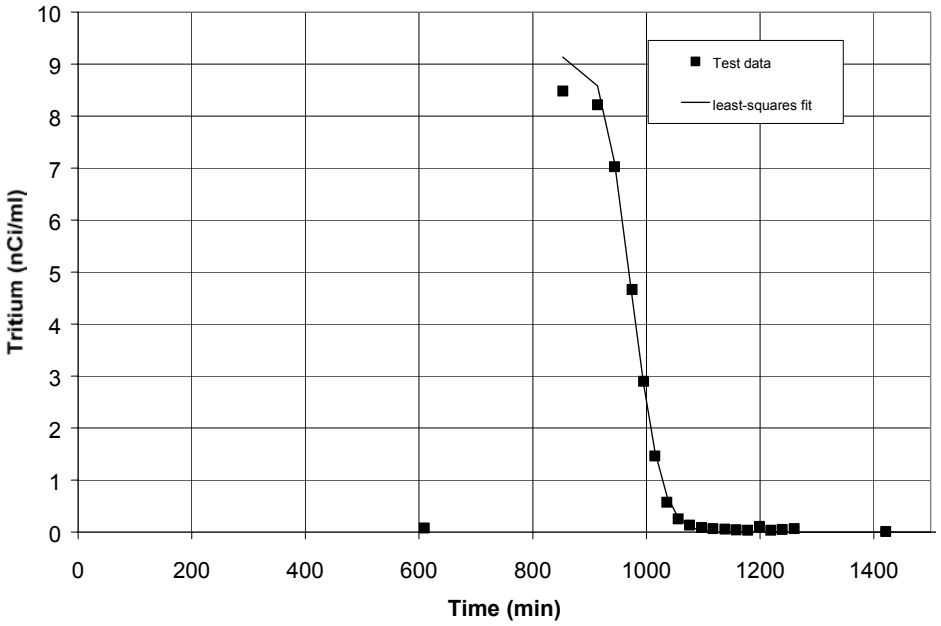

Figure 4. Breakthrough curve of tritium (symbols) for Test A and best-fit breakthrough curve determined using CXTFIT (line).

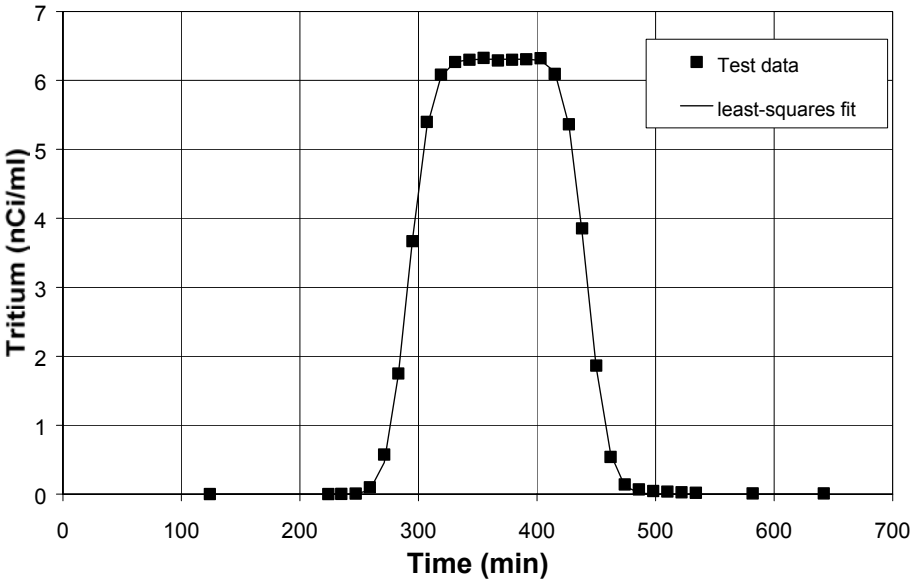

Figure 5. Breakthrough curve of tritium (symbols) for Test B and the best-fit breakthrough curve determined using CXTFIT (line).

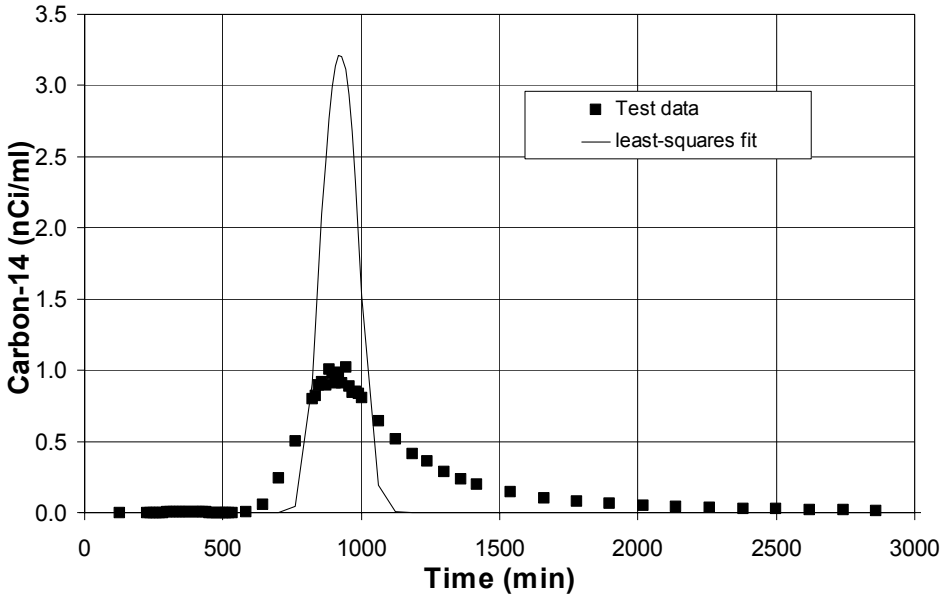

Figure 6. Plot of carbon-14 breakthrough concentrations (symbols) for Test B and a best-fit model using CXTFIT (line) assuming equilibrium, reversible adsorption of carbon-14 and physical transport properties determined from tritium transport.

Figure 6 shows that carbon-14 breakthrough for Test B occurs after about 900 minutes, compared to 300 minutes for tritium (Figure 5). These data are for the test conducted at a flow velocity of 0.105 cm/min. This indicates retardation of carbon-14 relative to tritium. Fitting a linear reversible sorption model using CXTFIT for carbon-14 transport gives a retardation factor of 3.20 ± 0.05 from which a K_d of 0.70 ± 0.02 ml/gm can be calculated using Equation 2. The experimental carbon-14 breakthrough data show a peak that is much more spread out than the equilibrium reversible sorption model can match. Therefore, other processes are taking place.

CXTFIT was used to fit a kinetic adsorption, two-site model to the carbon-14 breakthrough data from Test A (Figure 7) at a flow velocity of 0.045 cm/min. Physical transport properties were based on tritium breakthrough. Using the two-site, non-equilibrium model, parameters estimated using CXTFIT along with the 95% confidence interval for the estimate gave a retardation factor of 3.78 ± 0.05, a K_d of 0.89 ± 0.02 ml/gm, a fraction of sites that maintain equilibrium with the solution of 59% ± 1.3% and a rate coefficient for adsorption of 0.0033 ± 0.0003 min^{-1}. Additional models were fit by adding additional parameters for degradation and generation of carbon-14 on adsorption sites. Better fits were obtained by adding additional parameters. However, additional mechanisms do not seem justified as there are no sources or sinks of carbon-14 in the column.

Test B (Figure 8) at a flow velocity approximately twice the velocity of Test A was also conducted on the column. Physical transport properties were again based on tritium breakthrough. Using the two-site, non-equilibrium model, parameters estimated using CXTFIT along with the 95% confidence interval for the estimate gave a retardation factor of 3.40 ± 0.05, a K_d of 0.77 ± 0.02 ml/gm, a fraction of sites that maintain equilibrium with the solution of 56% ± 2%, and a rate coefficient for adsorption of 0.0097 ± 0.0013 min^{-1}.

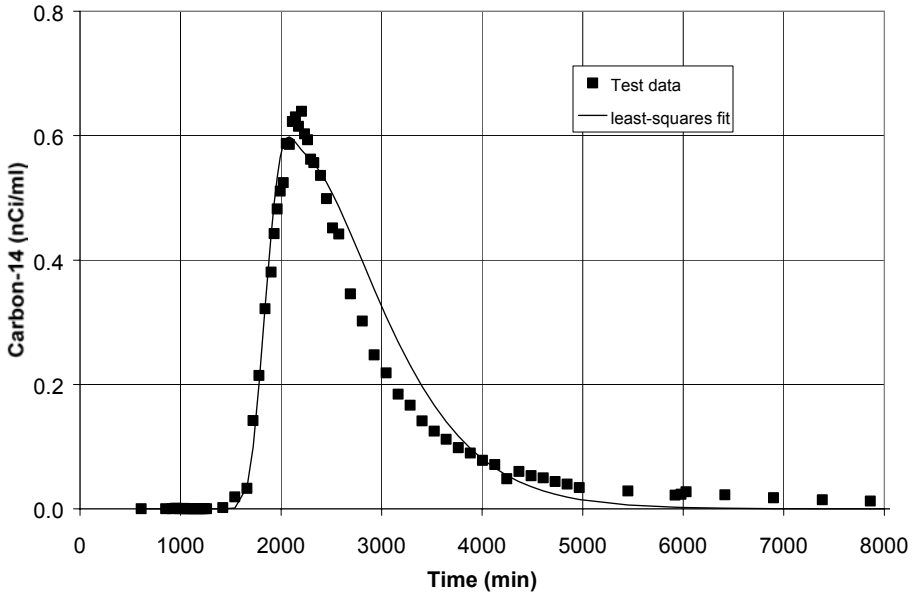

Figure 7. Plot of carbon-14 breakthrough concentrations for Test A (symbols) and a best-fit model (line) using a two-site kinetic adsorption model. Advective velocity and dispersion fixed by tritium.

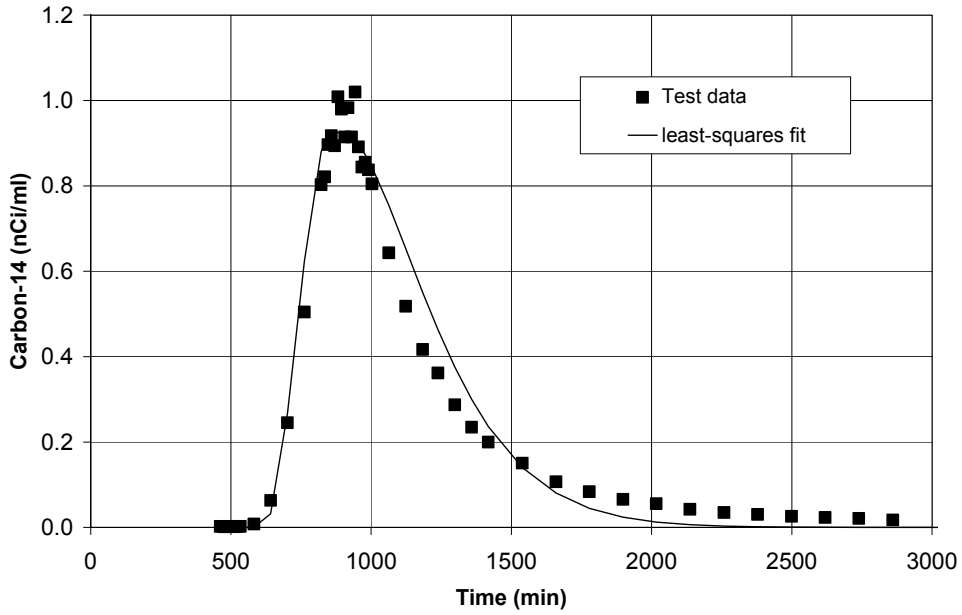

Figure 8. Plot of carbon-14 breakthrough data (symbols) from Test B and a best fit curve using CXTFIT (line) using a two site, kinetic adsorption model. Advective velocity and dispersion determined from the tritium breakthrough curve.

The dimensionless rate term, ω, is fit to the data and the rate coefficient for adsorption is calculated from Equation 6. The value of ω determined from Test A was 2.58 ± 0.21 for a 95% confidence interval of 2.37 to 2.79; and from Test B was 2.97 ± 0.33 for a 95% confidence interval of 2.64 to 3.30. There is no significant difference in the dimensionless rate constants determined for the two experiments at the

95% confidence level. The difference in dimensional rate coefficients (ratio 2.3) mainly compensates for the different velocity (ratio 2.9) in the two experiments. Therefore, while the two-site model of adsorption provides a better fit to the data, the inability to derive a single rate coefficient from the two experiments indicates that the adsorption mechanism does not include a kinetic rate process.

The linear K_d assumes that there is a linear relation between the concentration in solution and the adsorbed concentration. However, not all adsorption sites have the same binding energy, and there are a finite number of adsorption sites available. Therefore, there is not always a linear relation between adsorbed and solution concentrations. A Freundlich isotherm is used to model nonlinear adsorption behavior (Fetter 1993). A Freundlich isotherm is expressed as:

$$C_s = K_f C_l^n \tag{17}$$

where

K_f = Freundlich distribution coefficient

n = constant.

As n approaches 1, sorption approaches linearity and K_f approaches the linear K_d.

The shape of the breakthrough curve of a solute that follows a Freundlich isotherm with n less than 1 is steep on the upswing with a long drawn-out tail on the downswing side of the breakthrough. In contrast, the breakthrough curve of a solute that follows a linear isotherm is symmetrical. Inverse modeling of carbon-14 column experiments was performed to estimate Freundlich sorption isotherm parameters. The PORFLOW groundwater modeling software (ACRi 2000) was used to simulate flow and transport in the experiment columns, and the UCODE inverse model (Poeter and Hill 1998) was used to optimize the Freundlich isotherm parameters simulated by the PORFLOW software.

The PORFLOW software is a general purpose tool for simulating fluid flow, heat, and mass transport in porous or fractured media. The governing equation for solute interaction with porous matrix is formulated within PORFLOW using a linear sorption isotherm equation (Equation 1). However, PORFLOW allows the partition coefficient (K_d) to be specified as a non-linear function of solute concentration. This allows the Freundlich isotherm (Equation 17) to be simulated as

$$C_s = K_f C_l^{n-1} C_l \tag{18}$$

in which the K_d term is replaced by $K_f C_l^{(n-1)}$. The only drawback to using this alternative formulation of the Freundlich isotherm is that solute concentrations can never be zero when n values are less than 1. This problem is easily solved by specifying a very small background solute concentration within the PORFLOW simulation.

The UCODE software is a general purpose inverse model, which can run any application model or set of models that use ASCII input and output files. The UCODE inverse model uses non-linear regression to optimize any specified application model parameters to observed data. UCODE solves the non-linear regression problem by minimizing a weighted least-squares objective function with respect to the optimized parameter values using a modified Gauss-Newton method.

Freundlich isotherm parameters estimated by fitting the laboratory column data are shown in Table 5. The parameters estimated from the two tests are not significantly different at the 95% confidence level. In

Figure 9, computed breakthrough from the column using a Freundlich isotherm with a K_f of 0.508 and an exponent n of 0.457 is compared to the data from Test B. Computed breakthrough for the two-site model based on the CXTFIT parameters is included for comparison. The arrival curve of the laboratory carbon-14 data is earlier than predicted by the Freundlich isotherm. The peak heights and flushing curves are well matched by the Freundlich isotherm. The two-site model provides a very good match to the arrival curve of the carbon-14 laboratory data, but does not match the shape of the flushing curve. A computed Freundlich breakthrough curve and a computed two-site model breakthrough curve are compared to the laboratory carbon-14 breakthrough data for Test A in Figure 10. The curve shows the same relative behavior to breakthrough from Test A as from Test B. Neither the two-site, nonequilibrium adsorption conceptual model, nor the Freundlich, nonlinear adsorption isotherm conceptual model, explain all aspects of the carbon-14 breakthrough curve. The arrival portion of the breakthrough curve seems to be fit best by the equilibrium adsorption conceptual model. The flushing portion of the carbon-14 breakthrough curve seems to be fit best by a nonlinear adsorption isotherm.

Table 5. Freundlich isotherm parameters estimated by inverse modeling of the carbon-14 breakthrough data from the laboratory columns.

	Best estimate	95% lower confidence limit	95% upper confidence limit
Test A			
n	0.479	0.453	0.506
K_f	0.499	0.483	0.514
Test B			
n	0.457	0.424	0.490
K_f	0.508	0.485	0.531

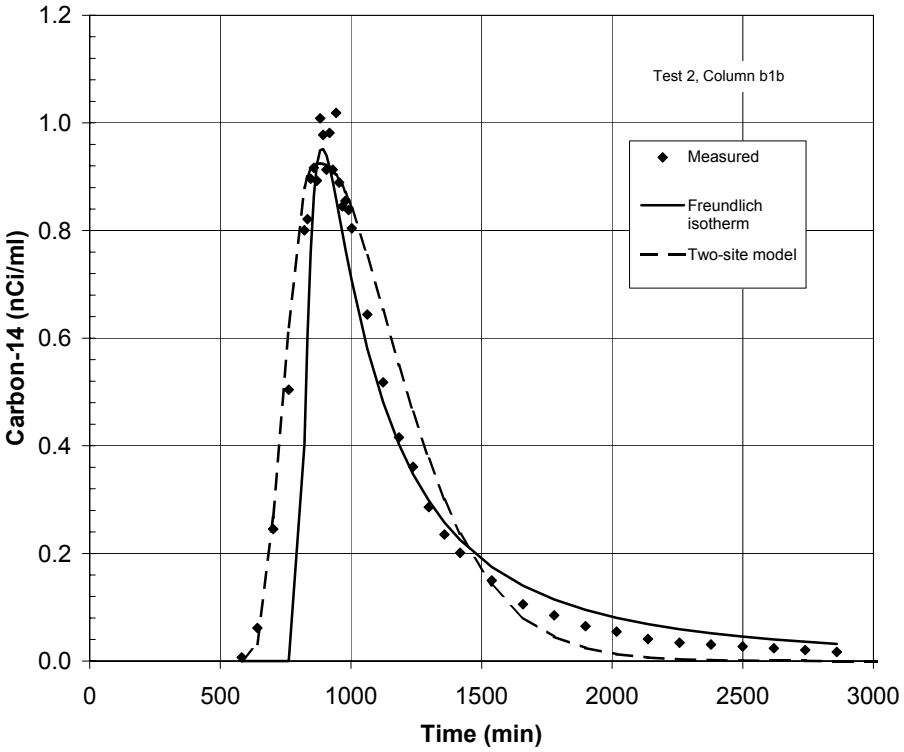

Figure 9. Plot of a Freundlich isotherm (solid line) fit to the carbon-14 breakthrough curve (symbols) for Test B compared to the CXTFIT result for the two-site conceptual model.

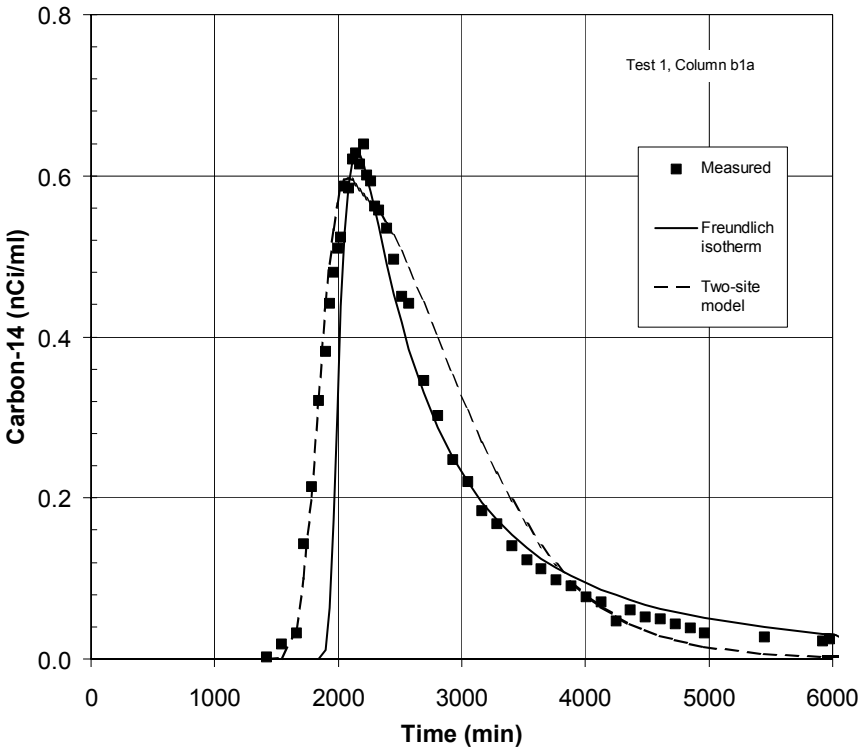

Figure 10. Plot of a Freundlich isotherm (solid line) fit to the carbon-14 breakthrough curve (symbols) for Test A compared to the CXTFIT result for the two-site conceptual model.

Based on the fits of various equations to the carbon-14 breakthrough data, no definitive model for adsorption has been derived. Additional work is needed to study the number and types of adsorption sites for carbon-14 on sediments. From the models, there appear to be two types of adsorption sites. One type of site is a reversible, equilibrium adsorption site. The second type of site may be a non-linear, reversible adsorption site. Column studies indicate that most of the carbon-14 left the column indicating that adsorption is reversible for residence times on the order of hours. The experimental results do not support the presence of a kinetic adsorption site.

The range of carbon-14 distribution coefficients determined from the laboratory column experiments (0.77 and 0.89 ml/g) are consistent with the range of distribution coefficients measured by Dicke and Hohorst (1997) for SDA sediments (0.1 to 2.0 ml/g). Uncertainties with recovery of tracer and carryover between experiments will have little effect on the timing of the peak of the breakthrough curve for carbon-14. The retardation factor, and therefore the distribution coefficient, is primarily dependent on the timing of the peak.

3.4 Diffusion

Gas diffusion experiments were run on Spreading Area B sediment to measure the tortuosity of the sediment. A conservative tracer gas, sulfur hexafluoride, was used to measure tortuosity. Experiments were also conducted with carbon dioxide. The photoacoustic analyzer altered the concentration of carbon dioxide when the gas was recycled through the reservoir and the analyzer, so the carbon dioxide data could not be used.

3.4.1 Experimental Materials

Gas diffusion experiments were conducted in a Plexiglas column 24.1 cm long and 5 cm in diameter (Figure 11). The column was packed with air-dried Spreading Area B sediment. Sediment was sieved through an 850 micrometer sieve to remove larger particles and organic debris. Sediment was added to the column in 2.5 cm lifts. Each lift was compacted before the next lift was added. The Plexiglas column was weighed before and after filling with sediment to obtain the mass of sediment added to the column. Bulk density was calculated as the mass of added sediment divided by the volume of the column. The bulk density of the column used for the diffusion experiments was 1.38 g/cm^3 with a porosity of 0.49 cm^3/cm^3. A sample of the air-dried sediment was further dried to constant weight at 104ºC to determine the residual moisture content. The sediment lost 0.0165 g of water per g of sediment for a volumetric water content of 0.023 cm^3/cm^3.

Gas diffusion experiments were conducted with carbon dioxide and sulfur hexafluoride. Gas analyses were performed with a photoacoustic infrared multigas analyzer. The gas analyzer cycles gas from the source chamber through the analyzer and back into the source chamber. There should be no loss of gas as there would be if gas was extracted from the source chamber for analysis.

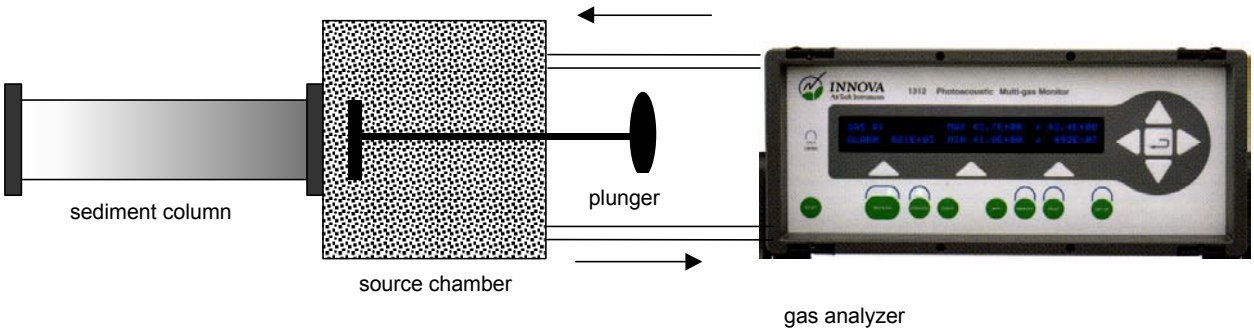

Figure 11. Experimental apparatus for measuring diffusion coefficients in sediments.

3.4.2 Experimental Conditions

Gas diffusion experiments were conducted using a nonsteady-state configuration. The apparatus for the gas diffusion experiments is shown in Figure 11. One end of the packed sediment column was attached to the source reservoir at atmospheric pressure, and a plunger closed to isolate the column from the reservoir. The other end of the sediment column was vented to the atmosphere to give a constant concentration boundary condition at that end. The source reservoir was then filled with a mixture of air, carbon dioxide, and sulfur hexafluoride. The source reservoir was connected to the photoacoustic gas analyzer. The gas analyzer circulated gas from the source reservoir for analysis. This helped mix the gas in the source reservoir maintaining a well mixed boundary condition. It also permitted analysis of the composition of the source reservoir without affecting the pressure of the source reservoir.

When the source reservoir was well mixed, the plunger was opened, connecting the source reservoir and the sediment column. The concentration of tracer gases in the source reservoir decreased over time as the tracers diffused through the sediment column to the atmosphere, and air diffused back through the column to the source reservoir.

All gas diffusion experiments were conducted on the same packed column of sediment. Between experiments, filtered laboratory air was pumped through the column to purge the tracer gases. Effluent from the column was tested using the gas analyzer to assure that the column was well purged prior to the next experiment.

3.4.3 Data Reduction

The time rate of change of the tracer composition in the source reservoir was used to determine the diffusion characteristics of the Spreading Area B sediment. For the physical configuration of the experimental apparatus, the solution to the diffusion equation is given by (Currie 1960a):

$$\frac{c}{c_0} = \sum_{i=1}^{\infty} \frac{2h \exp\left(-D_{eff} \eta_i^2 t\right)}{L\left(\eta_i^2 + h^2\right) + h} \tag{19}$$

After a short period, only the first term of the summation remains significant, and Equation 19 can be reduced to:

$$\frac{c}{c_0} = \frac{2h \exp\left(-D_{eff} \eta_1^2 t\right)}{L\left(\eta_1^2 + h^2\right) + h} \tag{20}$$

where

c = gas concentration (mg/kg) at time = t

c_0 = initial gas concentration (mg/kg) at time = 0

h = θ_g/a (cm^{-1})

η_i = roots of the equation [$\eta \tan(\eta L) = h$] (cm^{-1})

L = length of the column (cm)

t = time (min)

D_{eff} = effective gas phase diffusion coefficient in the soil gas (cm^2/min)

The first positive root (η_1) was determined using the Solver add-in in Microsoft Excel. The equation for η_1 was rearranged to yield:

$$\frac{a}{\theta_g}\eta_1 \tan(\eta_1 L) = 1 \qquad (21)$$

where

θ_g = air-filled porosity (cm^3/cm^3)

a = length of the source chamber (cm)

Equation 21 was entered into the target cell in the spreadsheet with a criteria to find the value of η_1 that would give a value of 1 for the equation. Convergence was confirmed by reaching the root from both directions.

A plot of ln(c) against t gives a straight line with a slope of $-D_{eff}\eta_1^2$ after a short period of diffusion from the source chamber. From the slope of the line and geometric information about the system, the effective molecular diffusion coefficient was calculated. This coefficient is the effective diffusion coefficient, D_{eff}, for the column of Spreading Area B sediment. The tortuosity of the air-dried sediment was calculated from the effective diffusion coefficient measured in the column and the free air diffusion coefficient of the gas using Equation 7.

3.5 Diffusion in the Gas Phase

Gas phase diffusion tests were conducted to determine the relation between porosity and diffusion in dry Spreading Area B sediment. The upward diffusion of volatile compounds including carbon dioxide and volatile organic compounds is an important release pathway from waste buried at the SDA. The cap material at the SDA is Spreading Area B material similar to that used in these experiments.

Diffusion coefficients for carbon dioxide and sulfur hexafluoride into air were calculated using the Fuller, Schettler, and Giddings relation and data given in Perry, Green, and Maloney (1984):

$$D_{air} = \frac{10^{-3} T^{1.75} \left[\frac{1}{M_g} + \frac{1}{M_{air}} \right]^{1/2}}{P \left[\left(\sum v \right)_g^{1/3} + \left(\sum v \right)_{air}^{1/3} \right]^2} \quad (22)$$

where

T = temperature (K)

M = molecular weight of air and the tracer gas (g/mole)
28.8 for air, 146 for SF_6, 44 for CO_2

P = atmospheric pressure (atm)

v = atomic diffusion volumes (cm^3)
20.1 for air, 69.7 for SF_6, and 26.9 for CO_2

D_{air} = diffusion coefficient for the tracer gas into air (cm^2/sec)

For laboratory conditions of temperature equal to 23ºC and air pressure equal to 0.835 atm the diffusion coefficient for carbon dioxide is calculated to be 11.1 cm^2/min and 6.6 cm^2/min for sulfur hexafluoride.

Five diffusion experiments were run in the sediment column. Figure 12 shows the reduced concentration of sulfur hexafluoride in the source chamber as a function of time. For all five experiments, the change in sulfur hexafluoride concentration with time is very similar. To calculate the gas phase diffusion coefficient, the source chamber concentration data were transformed by taking the natural log of the concentration. Sulfur hexafluoride (Figure 13) shows a very good linear slope in terms of ln(concentration) with time after about 150 min. Using the slopes of the decline in ln(concentration) with time, the sediment column diffusion coefficient for sulfur hexafluoride was calculated to be 2.08 ± 0.10 cm^2/min with the calculated diffusion coefficient in five experiments ranging from 1.82 to 2.24 cm^2/min. The model fits the sulfur hexafluoride data well (Figure 14).

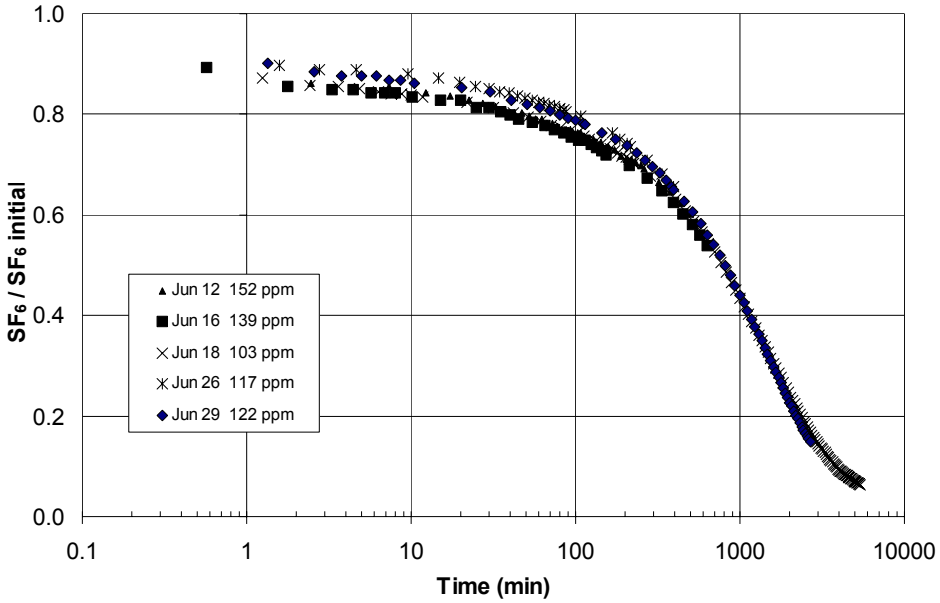

Figure 12. Source chamber sulfur hexafluoride concentrations for all diffusion experiments.

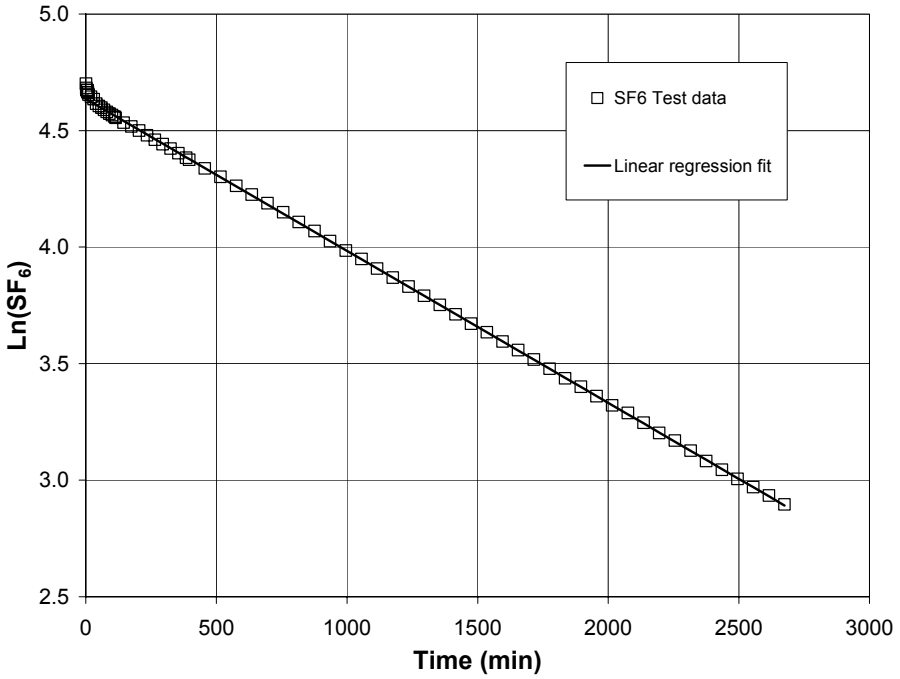

Figure 13. Plot of sulfur hexafluoride concentration in the source reservoir as a function of time for the test conducted June 29 and the fit of a linear regression to the data.

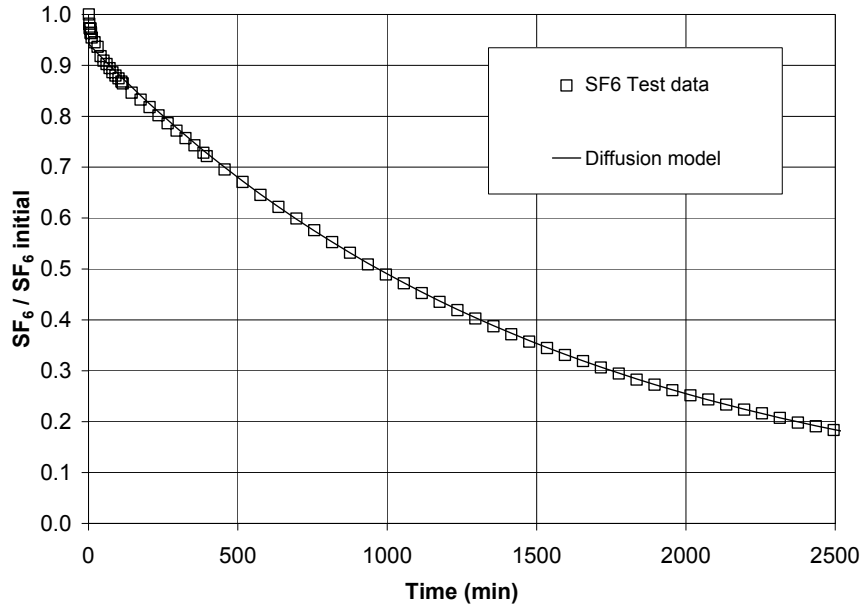

Figure 14. Fit of diffusion model wit D_m = 2.08 cm^2/min to sulfur hexafluoride test data collected June 29.

The measured effective sulfur hexafluoride diffusion coefficient can be used to estimate the tortuosity of the sediment. Using Equation 7, the tortuosity of the sediment is calculated from the ratio of the diffusion coefficient in air to the measured gas phase diffusion coefficient (6.6/2.08) to be 3.17. The relation between tortuosity and air-filled porosity can be calculated by rearranging Equation 10 and solving for *m-n*.

$$m - n = \frac{\ln\left(D_{eff} / D_{air}\right)}{\ln\left(\theta_t\right)} \tag{23}$$

Substituting 0.49 for the air-filled porosity (measured porosity in this case), and a ratio of measured air to sediment diffusion coefficients of 2.08/6.6, and solving for *m-n* gives a value of 0.6. Currie (1960b) performed diffusion experiments on a wide range of materials to evaluate the exponent *m-n* in Equation 10. He found that the exponent *m-n* ranged from 0.4 for sands to as much as 10 for powdered mica and vermiculite. Sand and mixtures of sand-sized particles had an *m-n* of about 0.4 to 0.6. Soils had a value of *m-n* of about 1. Clays and mixtures of clays had an *m-n* of about 2. The Spreading Area B sediment, with a composition of silty-clay and an *m-n* of 0.6, is consistent with these experimental results. Therefore, the silty-clay sediments of the Spreading Area B material have a typical tortuosity for diffusion of gases through the air-filled pores. The difference between *m* and *n* for the Spreading Area B sediment is somewhat greater than for the usual empirical relations for soils (Table 1). Repeating Figure 1 with the addition of a new line with an *n* value of 2 and *m* of 2.6 (*m-n* = 0.6)(Figure 15) shows that upward diffusion through the cap material in the SDA may be somewhat less than predicted using the Millington parameters for Equation 9.

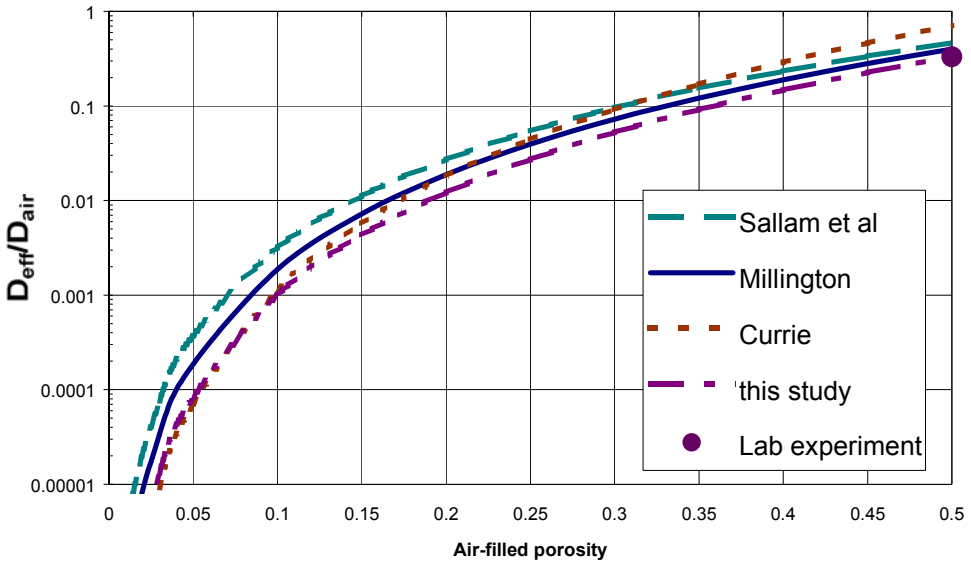

Figure 15. Change in effective diffusion coefficient for soil gas as a function of air-filled porosity.

Logarithms of the carbon dioxide concentration did not show a linear relation to time (Figure 17). Further tests were conducted to measure the carbon dioxide concentration in a source chamber that was sealed. Carbon dioxide concentrations decreased in the sealed chamber indicating a problem with using the photoacoustic gas analyzer to measure carbon dioxide in the closed loop system. The carbon dioxide data from these tests was not analyzed further.

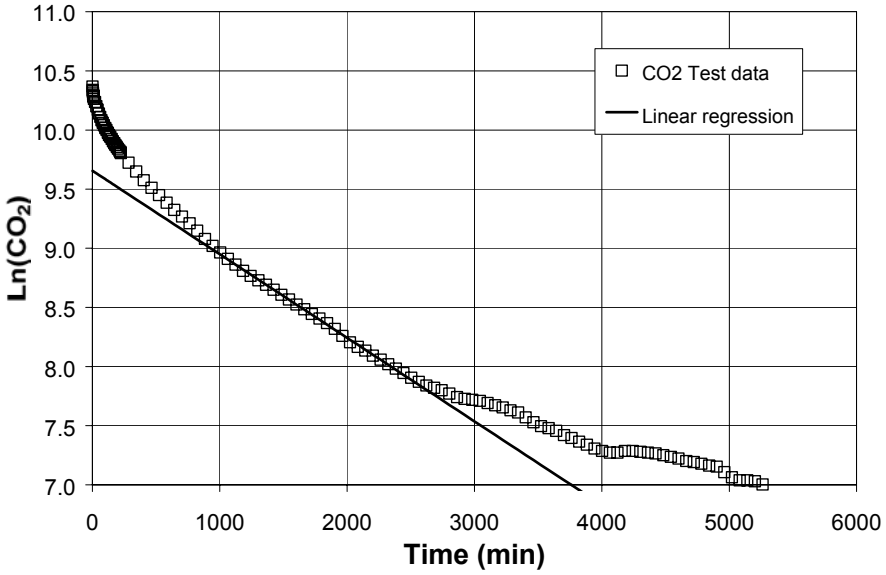

Figure 17. Plot of carbon dioxide concentration in the source reservoir as a function of time for the test conducted June 29, and one possible fit of a linear regression to a portion of the data between 500 and 2,700 minutes.

4. RESULTS AND DISCUSSION

The initial radiological performance assessment for the SDA (Maharas et al. 1994) did not include volatilization of carbon dioxide with diffusion in the gas phase nor did it include retardation by adsorption. Carbon-14 has been measured in the air above waste disposal sites inside the SDA (Ritter, McElroy, and Bhatt 1997). Field measurements show that gas-phase diffusion to the ground surface is an important pathway for gaseous radionuclides under some environmental conditions. Measurement of carbon-14 migration in columns, conducted in this investigation, show that carbon-14 will migrate more slowly than infiltrating water by a factor of about 3.6. The implications for transport of radioactive carbon to the aquifer are discussed in this section.

Simple calculations can be performed to assess the impacts of these processes on the migration of carbon-14. Diffusion to the atmosphere will reduce the total activity of carbon-14 that is available for transport to the aquifer. Retardation by adsorption to the rocks in the vadose zone will permit a small amount of radioactive decay. The vadose zone beneath the SDA consists of interbedded layers of basalt and sediments. Material properties vary widely between layers. No attempt will be made to mimic the subsurface structure. Only average properties are used to illustrate what the net effect of adsorption and volatilization could be.

The effective diffusion coefficient (Equation 9) and the apparent diffusion coefficient (Equation 12) can be used as a way to illustrate the relative importance of parameters and processes for predicting the migration of carbon-14 through the vadose zone at the SDA. The effective diffusion coefficient is calculated from the free air diffusion coefficient by including the effects of moisture content and tortuosity. In addition, the apparent diffusion coefficient includes partitioning to the soil water and the adsorption coefficient. Comparison of the effective and apparent diffusion coefficients calculated under a range of different conditions provides a way to quantify the relative effects of processes and subsurface conditions. The processes considered here are (1) diffusion in the gas phase, (2) partitioning between the gas phase and the vadose zone water phase, and (3) partitioning between the vadose zone water phase and the solid sediments. For gas phase diffusion the factors considered are (1) the functional relation of the sediment tortuosity to porosity, and (2) sediment moisture content. The Henry's Law constant for carbon dioxide partitioning to the vadose zone water phase is calculated from Equation 13. For partitioning to the sediment in the vadose zone, a linear partitioning coefficient (K_d) of 0.8 ml/g is used.

Calculations of the effective diffusion coefficient for a range of anticipated conditions at the SDA are shown in Table 6. In Table 6, effective diffusion coefficients are calculated for anticipated low and high moisture content conditions in SDA sediments using Equation 9 for two sets of parameters for *m* and *n*. The Millington parameters are those proposed by Millington (1959), and the parameters used in risk assessment calculations at the SDA are from Magnuson and Sondrup (1998). Based on the laboratory diffusion experiments in this investigation, alternative parameters are proposed where *m* and *n* differ by a value of 2.6. This is more consistent with parameters proposed by Currie (1960b) and results in a lower effective diffusion coefficient than the parameters proposed by Millington (1959).

In Table 7, apparent diffusion coefficients are calculated using Equation 12 to include the effects of mass transfer from the gas phase to the aqueous phase, and from the aqueous phase to the solid sediment. Mass transfer further reduces diffusion in the gas phase by decreasing the mass that remains in the gas phase.

Table 6. Effective gas-phase diffusion coefficient of carbon dioxide in the SDA calculated for different soil-moisture content and different relations between moisture and tortuosity, with total porosity equal to 0.45 and a free air diffusion coefficient of 16,000 cm^2/day.

Gas-phase diffusion coefficient (cm^2/day)	Dry conditions ($\theta_g = 0.25$)	Wet conditions ($\theta_g = 0.10$)
$D_{eff} = D_{air}(\theta_g^{2.33}/\theta_t^2)$ (Millington parameters)	3109	370
$D_{eff} = D_{air}(\theta_g^{2.6}/\theta_t^2)$ (this study)	2147	200

Table 7. Calculated apparent gas-phase diffusion coefficients incorporating both tortuosity effects and the capacity factor, which accounts for partitioning of carbon dioxide from the gas phase to vadose zone water and sediments.

Apparent diffusion coefficient (cm^2/day)	Dry conditions	Wet conditions	
$D_{app} = D_{eff}$/Capacity factor, no adsorption	270	7.8	Millington
$D_{app} = D_{eff}$/Capacity factor, no adsorption	186	4.2	this study
$D_{app} = D_{eff}$/Capacity factor with adsorption	42	1.8	Millington
$D_{app} = D_{eff}$/Capacity factor with adsorption	30	1.0	this study

As conditions change from wet to dry, the apparent diffusion coefficient changes by a factor of 23 to 30 depending on the values of the other parameters. Using the tortuosity value measured in this study for diffusion in the soil gas phase, rather than the Millington parameters, has very little effect on the effective diffusion coefficient with maximum effect of about a factor of 2 under wet conditions. Including partitioning of carbon dioxide to the soil aqueous phase (with a K_d of zero) reduces the effective diffusion coefficient by a factor of 12. Adding partitioning to the solid phase (including a $K_d = 0.8$ ml/g) reduces the effective diffusion coefficient by a factor of 75 in dry soil and a factor of 200 in wet soil. Based on these comparisons, the most important process to quantify is the partitioning of carbon dioxide to the solid sediment. Second most important is to accurately measure the moisture regime in the subsurface at the SDA and correctly incorporate the temporal variations in that regime into a computer simulation. The variation in soil tortuosity to diffusion as a function of moisture content, plays a less significant role.

A simple explicit finite difference solver in one dimension (Appendix C) was used to simulate the gas-phase diffusion and dissolved-phase advection of carbon dioxide in the vadose zone under the SDA to further assess the important processes and subsurface conditions. The simple calculation of an effective or apparent diffusion coefficient does not address interactions between advection and diffusion. Steady-state conditions for all hydraulic properties were assumed and an initial mass of carbon dioxide was located between 1.5 and 6 meters below ground surface. Table 8 shows the hydraulic parameters used in the simulation based on moisture monitoring data collected at the SDA by Bishop (1998). A Henry's Law constant of 0.076 from Equation 13 and a partition coefficient (K_d) of 0.8 ml/g from the laboratory experiments were used in the simulations.

Table 8. Vadose zone properties at the subsurface disposal area for dry and wet conditions (Bishop 1998).

Parameter	Dry conditions	Wet conditions
Water flux (cm/year)	0.9	2.3
Darcy flux (cm/day)	2.5E-3	6.3E-3
Pore velocity (cm/day)	1.2E-2	1.8E-2
Moisture content	0.20	0.35
Air-filled porosity	0.25	0.10

For the conditions used in the performance assessment, no carbon-14 was transported to the atmosphere. The only process considered was advection downward to the aquifer. For the conditions considered here, the maximum loss of carbon-14 to the atmosphere was calculated to be 15% in the case with dry sediment, effective diffusion calculated from the Millington parameters, and no adsorption onto sediments (). Any other combination of parameters reduced the loss of carbon-14 to the atmosphere. The maximum expected reduction in radioactive dose in the aquifer from carbon-14 is therefore from 5% to 10% including gas phase diffusion in the computer simulation.

Table 9. Percent of initial carbon dioxide in the source that is released to the atmosphere by diffusion over a period of seven years, as a function of transport parameters used in the simulation.

	$K_d = 0$ D_{eff} from Millington (m-n = 0.33)	$K_d = 0.8$ D_{eff} from Millington (m-n = 0.33)	$K_d = 0$ D_{eff} from this study (m-n = 0.6)	$K_d = 0.8$ D_{eff} from this study (m-n = 0.6)
Wet conditions	< 1%	< 1%	< 1%	< 1%
Dry conditions	15%	10%	6.5%	4%

The migration of a volatile contaminant, such as carbon-14, depends on the apparent diffusion coefficient. When the apparent diffusion coefficient is high, which occurs under dry conditions, the carbon-14 spreads throughout the vadose zone gas phase by diffusion and contaminant is lost to the atmosphere by diffusion. When the apparent diffusion coefficient is small, which occurs under wet conditions, the carbon-14 moves as a dispersed plug, advecting downward at the velocity of the infiltration. The calculated effect of adsorption onto sediments, shown in , leads to somewhat different conclusions than the calculations shown in Table 7. The most important information needed to predict the migration of carbon-14 is the moisture condition of the subsurface. The effect of adsorption and the tortuosity equation used are of less importance to determine the loss of carbon-14 to the atmosphere.

During downward advection through the vadose zone, adsorption of carbon-14 species on solid phases will retard the movement of carbon-14. The median residence time in the vadose zone under the SDA calculated by Magnuson and Sondrup (1998) was 130 years. In 130 years, carbon-14 (with a half-life of 5715 years) would decrease to 98.4% of the original release concentration due to radioactive decay. Unsaturated sediment in the vadose zone at the SDA will have a lower moisture content (about 0.25 cm^3/cm^3, [Magnuson and Sondrup 1998]) than the saturated sediments in the sediment column (0.46 cm^3/cm^3). The lower moisture content will have the effect of raising the retardation factor (Equation 2). For subsurface conditions at the SDA, the retardation factor for carbon-14 will be closer to five for a K_d of 0.8 ml/g. With a retardation factor of five and a water residence time of 130 years, the carbon-14 residence time would be on the order of 650 years. Radioactive decay in 650 years would only

reduce carbon-14 concentrations to 92% of the initial concentration. Carbon-14 has a long half-life relative to the residence time in the vadose zone, even when retardation is considered, so that radioactive decay does little to change the amount of carbon-14 reaching the aquifer.

5. CONCLUSIONS

Our experiments were successful in clarifying questions from the SDA radioactive performance assessment. These laboratory results produced parameters that can be used to predict the migration of carbon-14 in Spreading Area B sediment (used in SDA at RWMC). The studies included investigations in both the gaseous and aqueous phases. Diffusion experiments were conducted to determine the impact of tortuosity on the diffusion of carbon dioxide from the vadose zone to the atmosphere. Miscible displacement experiments were conducted to evaluate retardation of carbon-14 species by adsorption onto sediment.

Retardation of carbon-14 in sediment columns was used to determine that the distribution coefficient for carbon-14 on Spreading Area B sediment is in the range of 0.7 to 0.9 ml/g. This range is consistent with batch measurements of K_d on SDA sediments and values reported in the literature for natural sediments. A reversible, linear partition coefficient did not match the carbon-14 breakthrough data very well. The breakthrough of carbon-14 from the column was more spread out over time than could be explained by reversible, linear adsorption. Kinetic reactions do not account for this spreading. A Freundlich non-linear isotherm seemed to be the best model for the transport of carbon-14 through the sediment.

Diffusion experiments indicate that tortuosity factors for Spreading Area B sediment are somewhat higher than other sediment tortuosity factors in the literature. The overall effect of this would be to decrease the effective diffusion coefficient of the cap materials inside the SDA. The most important factor for predicting the migration of carbon-14 at the SDA is knowledge of the in situ soil moisture conditions, and changes in those conditions with time.

6. REFERENCES

ACRi, 2000, *PORFLOW User's Manual Version 4.00,* Analytical & Computational Research, Inc., Bel Air, Ca.

Allard, B., B. Torstenfelt, and K. Andersson, 1981, *Sorption Behavior of ^{14}C in Groundwater/Rock and Groundwater/Concrete Environments*, Report Prav 4.27, Department of Nuclear Chemistry, Chalmers University of Technology, Goteborg, Sweden.

ASTM, 1993, *Standard Test method for Distribution Ratios by the Short-Term Batch Method*, American Society for Testing and Materials, West Conshohocken, PA.

Barraclough, J. T., J. B. Robertson, and V. J. Janzer, 1976, *Hydrology of the Solid Waste Burial Ground, As Related to the Potential Migration of Radionuclides, Idaho National Engineering Laboratory*, IDO-22056, Open-File Report 76-471, U. S. Geological Survey, Idaho Falls, ID.

Bartholomay, Roy C., L. L. Knobel, and L. C. Davis, 1989, *Mineralogy and Grain Size of Surficial Sediment from the Big Lost River Drainage and Vicinity, with Chemical and Physical Characteristics of the Geologic Materials from Selected Sites at the Idaho National Engineering Laboratory, Idaho*, DOE/ID-22081, U. S. Geological Survey, Idaho Falls, ID.

Bartholomay, Roy C., 1990, *Mineralogical Correlation of Surficial Sediment from Area Drainages with Selected Sedimentary Interbeds at the Idaho National Engineering Laboratory, Idaho*, DOE/ID-22092, U. S. Geological Survey, Idaho Falls, ID.

Bethke, C. M., 1996, *Geochemical Reaction Modeling*, Oxford University Press, New York, NY.

Bishop, C. W., 1998, *Soil Moisture Monitoring Results at the Radioactive Waste Management Complex of the Idaho National Engineering Laboratory, FY-96, FY-95 and FY-94*, INEL/EXT-98-00941, Idaho National Engineering and Environmental Laboratory, Idaho Falls, ID.

Case, M. J., A. S. Rood, J. M. McCarthy, S. O. Magnuson, and B. H. Becker, 2000, *Technical Revision of the Radioactive Waste Management Complex Low-Level Waste Radiological Performance Assessment for Calendar Year 2000*, INEEL/EXT-2000-01089, Idaho National Engineering and Environmental Laboratory, Idaho Falls, ID.

Currie, J. A., 1960a, "Gaseous Diffusion in Porous Media Part 1. – A Non-Steady State Method," *British Journal of Applied Physics*, Vol. 11, pp. 314-317.

Currie, J. A., 1960b, "Gaseous Diffusion in Porous Media Part 2. – Dry Granular Materials," *British Journal of Applied Physics*, Vol. 11, pp. 318-324.

Dicke, Craig A., and F. A. Hohorst, 1997, *Carbon-14 Distribution Coefficients Measured from Batch Experiments on SDA Sediments*, INEEL/INT-98-00068, EDF-RWMC-1011, Idaho National Engineering and Environmental Laboratory, Idaho Falls, ID.

Fetter, C. W., 1993, *Contaminant Hydrogeology*, Macmillan Publishing Company, New York, NY.

Garnier, Jean-Marie, 1985, "Retardation of dissolved radiocarbon through a carbonated matrix," *Geochim. Cosmochim. Acta*, Vol. 49, pp. 683-693.

Gierke, J. S., N. J. Hutzler, and J. C. Crittenden, 1990, "Modeling the Movement of Volatile Organic Chemicals in Columns of Unsaturated Soil," *Water Resources Research*, Vol. 26, pp. 1529-1547.

Grathwohl, Peter, 1998, *Diffusion in Natural Porous Media*, Kluwer Academic Publishers, Boston, MA.

Harned, H. S., and F. T. Bonner, 1945, "The first ionization of carbonic acid in aqueous solutions of sodium chloride," *Jour. Amer. Chem. Soc*., Vol. 67, pp. 1026-1031.

Harned, H. S., and R. Davis Jr., 1943, "The ionization constant of carbonic acid in water and the solubility of carbon dioxide in water and aqueous salt solutions from 0 to 50 °C," *Jour. Amer. Chem. Soc.*, Vol. 65, pp. 2030-2037.

Harned, H. S., and S. R. Scholes, 1941, "The ionization Constant of HCO_3^- from 0 to 50 °C," *Journal of American Chemical Society*, Vol. 63, pp. 1706-1709.

Hull, L. C., M. N. Pace, and G. D. Redden, 1999, "Adsorption Parameters for Radioactive Liquid Waste Migration," *Scientific Basis for Nuclear Waste Management*, Materials Research Society Fall Meeting, Boston, MA.

Kreamer, David K., Edwin P. Weeks, and Glenn M. Thompson, 1988, "A Field technique to Measure the Tortuosity and Sorption-Affected Porosity for Gaseous Diffusion of Materials in the Unsaturated Zone With Experimental Results From Near Barnwell, South Carolina," *Water Resources Research*, Vol. 24, No. 3, pp. 331-341.

Lerman, A., 1988, *Geochemical Processes Water and Sediment Environments*, Robert E. Krieger Publishing Company, Malabar, FL.

Lide, D. R., 1994, *CRC Handbook of Chemistry and Physics*, CRC Press, Boca Raton, FL.

Magnuson, S. O., and A. J. Sondrup, 1998, *Development, Calibration, and Predictive Results of a Simulator for Subsurface Pathway Fate and Transport of Aqueous and Gaseous Phase Contaminants in the Subsurface Disposal Area at the Idaho National Engineering and Environmental Laboratory*, INEL/EXT-97-00609, Idaho National Engineering and Environmental Laboratory, Idaho Falls, ID.

Maheras, S. J., A. S. Rood, S. O. Magnuson, M. E Sussman, and R. N. Bhatt, 1994, *Radioactive Waste Management Complex Low-Level Waste Radiological Performance Assessment*, EGG-WM-8773, Idaho National Engineering and Environmental Laboratory, Idaho Falls, ID.

Martin, W. J., 1996, *Integration of Risk Analysis and Sorption Studies in the Subsurface Transport of Aqueous Carbon-14 at the Hanford Site*, Ph.D. Dissertation, Washington State University.

McCarthy, J. M., B. H. Becker, S. O. Magnuson, K. N. Keck, and T. K. Honeycutt, 2000, *Radioactive Waste Management Complex Low-Level Waste Radiological Composite Analysis*, INEEL/EXT-97-01113, Idaho National Engineering and Environmental Laboratory, Idaho Falls, ID.

Millington, R. J., 1959, Gas Diffusion in Porous Media, *Science*, Vol. 130, pp. 100-102.

Mozeto, A. A., P. Fritz, and E. J. Reardon, 1984, "Experimental Observation of Carbon Isotope Exchange in Carbonate-Water System," *Geochim. Cosmochim. Acta*, Vol. 48, pp. 495-504.

Nkedi-Kizza, P., J. W. Biggar, H. M. Selim, M. Th. van Genuchten, P. J. Wierenga, J. M. Davidson, and D. R. Nielsen, 1984, "On the Equivalence of Two Conceptual Models for Describing Ion Exchange During Transport Through an Aggregated Oxisol," *Water Resources Research*, Vol. 20, No. 8, pp. 1123-1130.

Perry, R. H., D. W. Green, and J. O. Maloney, 1984, *Perry's Chemical Engineers' Handbook, Sixth Edition*, McGraw-Hill Book Company, New York, NY.

Poeter, E. P. and M. C. Hill, 1998, *Documentation of UCODE, A Computer Code for Universal Inverse Modeling*, U.S. Geological Survey Water-Resources Investigations Report 98-4080.

Rightmire, Craig T., 1984, *Description and Hydrogeologic Implications of Cored Sedimentary Material from the 1975 Drilling Program at the Radioactive Waste Management Complex, Idaho*, DOE/ID-22067, U. S. Geological Survey, Idaho Falls, ID.

Rightmire, C. T., and B. D. Lewis, 1987, *Hydrogeology and Geochemistry of the Unsaturated Zone, Radioactive Waste Management Complex, Idaho National Engineering Laboratory, Idaho*, DOE/ID-22073, U. S. Geological Survey, Idaho Falls, ID.

Ritter, Paul D., D. L. McElroy, and R. N. Bhatt, 1997, *Beryllium Block Sampling Project Status for Fiscal Years 1995 and 1996*, INEL/INT-97-00094, Idaho National Engineering Laboratory, Idaho Falls, ID.

Sallam, A., W. A. Jury, and J. Letey, 1984, "Measurement of Gas Diffusion Coefficient under Relatively Low Air-Filled Porosity," *Soil Sci. Soc. Am. Jour.*, Vol. 48, pp. 3-6.

Simunek, Jiri, and D. L. Suarez, 1993, "Modeling of Carbon Dioxide Transport and Production in Soil 1. Model Development," *Water Resources Research*, Vol. 29, No. 2, pp. 487-497.

Solomon, D. K., and T. E. Cerling, 1987, "The Annual Carbon Dioxide Cycle in a Montane Soil: Observations, Modeling, and Implications for Weathering," *Water Resources Research*, Vol. 23, No. 12, pp. 2257-2265.

Striegl, R. G., and D. E. Armstrong, 1990, "Carbon dioxide retention and carbon exchange on unsaturated Quaternary sediments," *Geochim. Cosmochim. Acta*, Vol. 54, pp. 2277-2283.

Stumm, W. and J. J. Morgan, 1970, *Aquatic Chemistry*, John Wiley and Sons, Inc., New York, NY.

Suarez, D. L., and Jiri Simunek, 1993, "Modeling of Carbon Dioxide Transport and Production in Soil 2. Parameter Selection, Sensitivity Analysis, and Comparison of Model Predictions to Field Data," *Water Resources Research*, Vol. 29, No. 2, pp. 499-513.

Toride, N., F. J. Leij, and M. Th. van Genuchten, 1995, *The CXTFIT Code for Estimating Transport Parameters from Laboratory or Field Tracer Experiments*, Research Report No. 137, U. S. Salinity Laboratory, Riverside, CA.

Tullis, J. A., S. T. Marts, M. C. Pfeifer, and J. B. Sisson, 1993, *Corrosive Properties of Backfill Soils at the Radioactive Waste Management Complex, Idaho National Engineering Laboratory*, EGG-GEO-10382, Idaho National Engineering Laboratory, Idaho Falls, ID.

van Geen, Alexander, A. P. Robertson, J. O. Leckie, 1994, "Complexation of carbonate species at the goethite surface: Implications for adsorption of metal ions in natural waters," *Geochim. Cosmochim. Acta*, 58, pp. 2073-2086.

van Genuchten, M. Th., and P. J. Wierenga, 1976, "Mass Transfer Studies in Sorbing Porous Media I. Analytical Solutions," *Soil Sci. Soc. Am. Jour.*, Vol. 40, No. 4, pp. 473-480.

van Genuchten, M. Th., and R. J. Wagenet, 1989, "Two-Site/Two-Region Models for Pesticide Transport and Degradation: Theoretical Development and Analytical Solutions," *Soil Sci. Soc. Am. Jour.*, Vol. 53, No. 5, pp. 1303-1310.

Weeks, Edwin P., Douglas E. Earp, and Glenn M. Thompson, 1982, "Use of Atmospheric Fluorocarbons F-11 and F-12 to Determine the Diffusion Parameters of the Unsaturated Zone in the Southern High Plains of Texas," *Water Resources Research*, Vol. 18, No. 5, pp. 1365-1378.

Zachara, J. M., D. C. Girvin, R. L. Schmidt, and T. Resch, 1987, "Chromate Adsorption on Amorphous Iron Oxyhydroxide in the Presence of Major Groundwater Ions," *Environmental Science and Technology*, Vol. 21, p. 589.

Appendix A

Evaporation of Water from Sample Tubes

Appendix A
Evaporation of Water from Sample Tubes

Purpose

The purpose of this experiment was to measure the evaporation of water from sample collection tubes during the sampling of column effluent using a fraction collector. These losses will be evaluated for their impact on the miscible displacement experiments conducted using laboratory columns and other work.

Approach

Evaporation was evaluated over a period of 19 hours using an Eldex Universal Fraction Collector with an Eldex U-200 test tube rack and 16 x 100 mm Fisherbrand Borosilicate Disposable Culture Tubes. The tubes were weighed before the test. Water was added to the tubes at approximately 0.9 mL/hr with the tubes being rotated at once per hour. The test was concluded after19 hours, and the tubes weighed. The first tube filled had been open to evaporation for 18 hours. The last tube filled was not given any time for evaporation. The difference in weight between the empty tubes and tubes with water were correlated to the time since they had been filled.

Results

The results of the weight loss experiments are shown in Figure A-1. Most of the data fall along a line that shows a gradual, linear weight loss from the sample tubes over time. There is a second group of data that indicate a second linear trend. The conclusion is that the same volume of water was not delivered to each of the tubes. For a few of the tubes, the volume added was slightly less. To add 0.9 ml of water to a tube over an hour, one drop more or less would make an appreciable difference. A linear regression of the data in the upper group provides an evaporation value of 0.0035 ± 0.001 mL/hr with an R^2 value of 0.98.

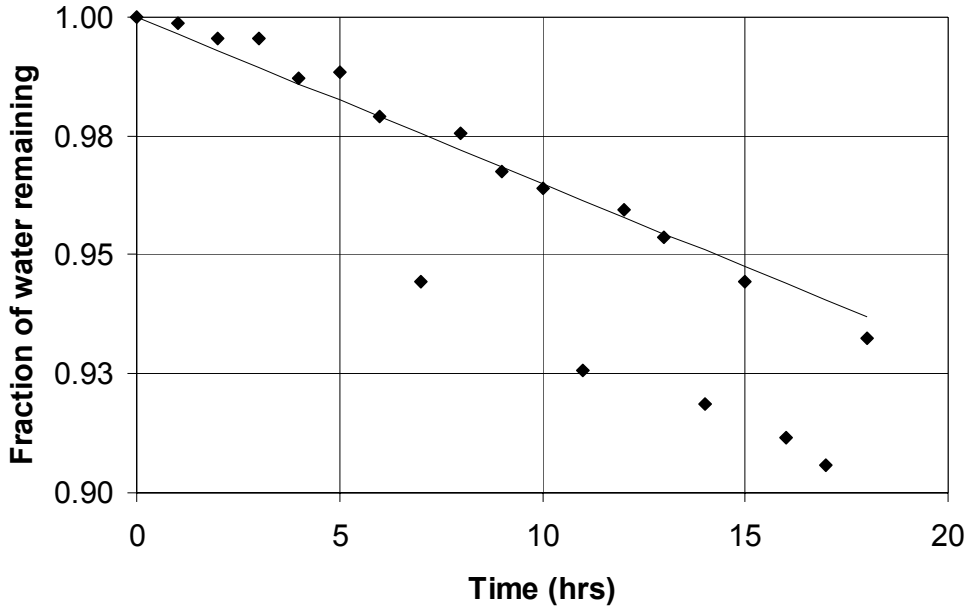

Figure A-1. Water lost from sample collection tubes by evaporation measured by weight loss.

Appendix B

Losses of Carbon-14 during Sample Collection

Appendix B
Losses of Carbon-14 during Sample Collection

Purpose

The purpose of this work was to measure the losses of carbon-14 that result from the sampling of column effluent, which has been tagged with carbon-14 as carbonate, using a fraction collector. These losses will be evaluated for their impact on the miscible displacement experiments conducted using laboratory columns and other work.

Equipment

An experimental setup, which filled and stored a collection tube while passing oil-free instrument air over and around the collection tube, was constructed in the IRC Model Shop from Plexiglas™ (Figure B-1). The setup also mimicked the mixing processes which occur in collection tubes on the fraction collector. The carrier air would pick up any $^{14}CO_2$ that exsolved from the collection tube and carry it, through narrow bore tubing (to minimize back diffusion), into a midget glass impinger. In the impinger, any $^{14}CO_2$ present was absorbed by the ethanol-ethanolamine absorbent.

The full setup (shown schematically in Figure B-2) was assembled and operated in the radiological buffer area in IF-603, Laboratory A17. Two trains were operated as duplicate experiments.

Reagents

Synthetic ground water was prepared from reagent grade chemicals and MilliQ™ water. Its final composition is reported in the body of the report. Carbon-14 was obtained as a sodium carbonate solution from Amersham (Product Code CFY.44) containing 2.863 E+6 disintegrations per minute of ^{14}C per gram of solution. The overall uncertainty in the radioactive measurement is 1.7%.

Air Flow

Air flow through the apparatus came from the 240 kPa building instrument air. As supplied, it is "oil-free," but still contains "ambient" carbon dioxide at an estimated level of 360 – 400 ppmv. Supply pressure variability was stabilized by passing the building air into a regulator whose output pressure was set to 138 kPa. The air flow was split with each half passing through a control valve and a rotameter before entering the Plexiglas™ chamber. The flow was adjusted to about 230 cc min^{-1} for all trains in all runs. At ambient temperature and pressure, this flow corresponds to about 180 std cc min^{-1}. The calculated superficial face velocity across the mouth of the centrifuge tube is about 17 cm min^{-1}.

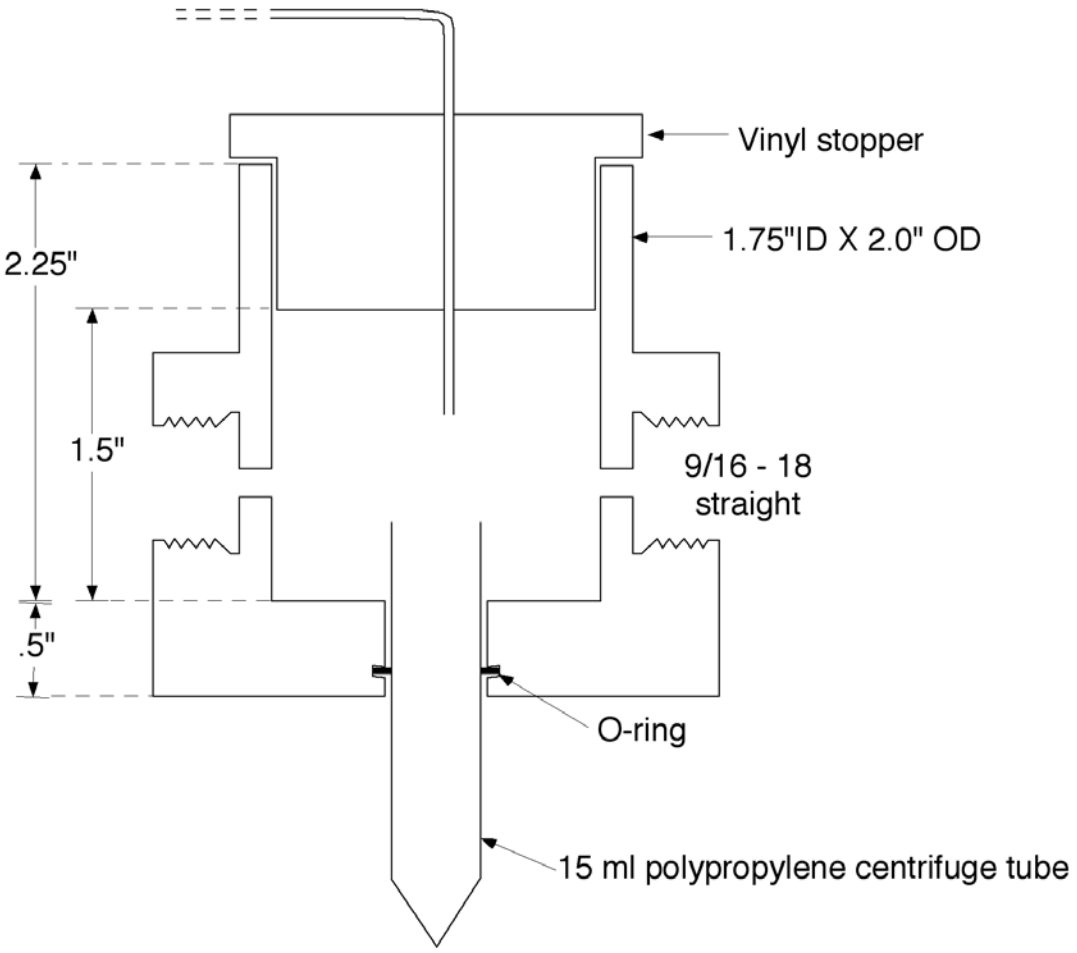

Figure B-1. Schematic diagram of the flow-through chamber used to measure the loss of carbon-14 from fraction collector tubes.

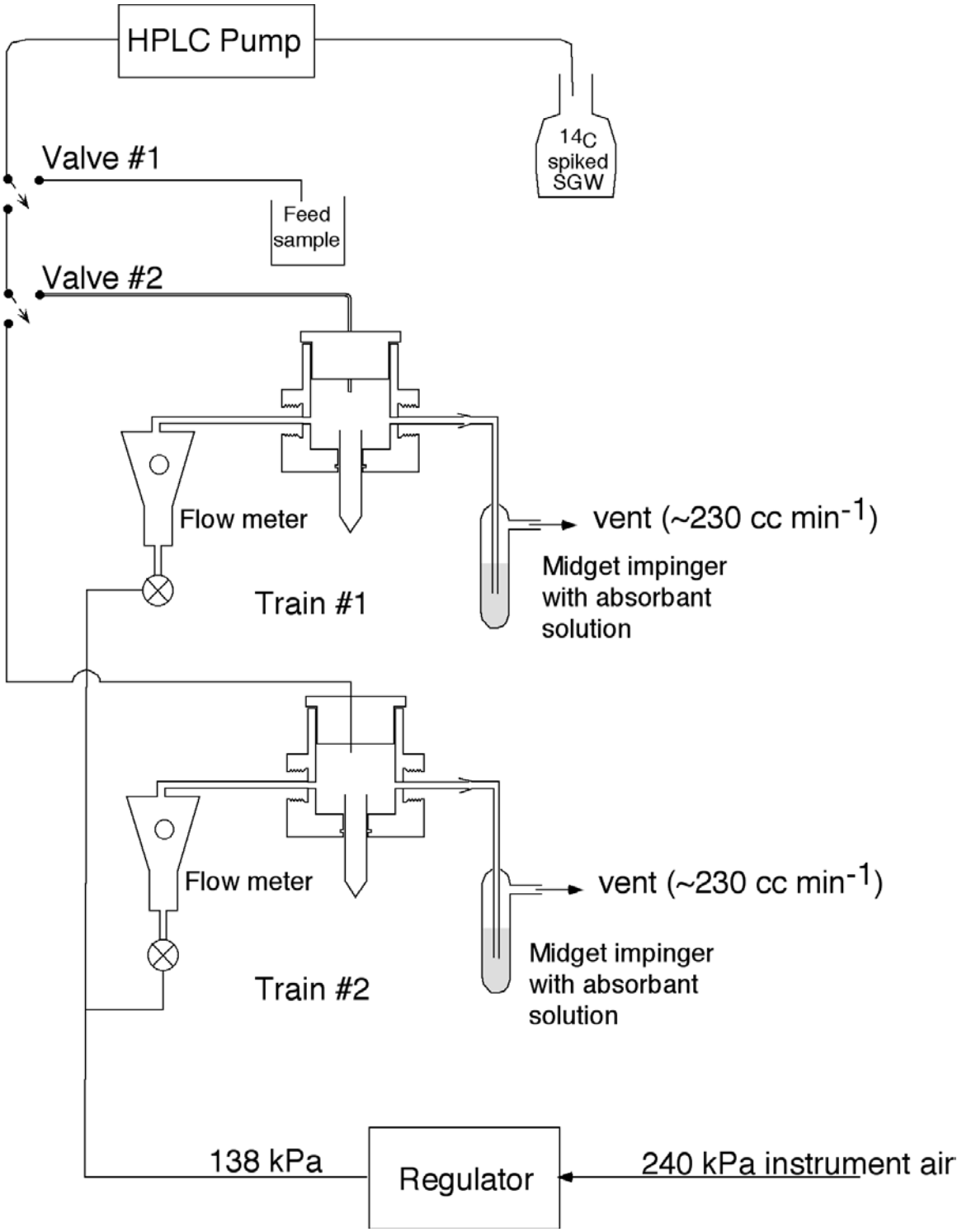

Figure B-2. Schematic diagram of the experimental apparatus and support equipment used to measure the loss of carbon-14 from fraction collector tubes.

Temperature Control

Customary building temperature control was used during the course of these experiments. Data logging permitted examination of room temperature at 10 minute intervals. The results are summarized in Table B-1.

Table B-1. Room temperature during volatilization experiments.

Run Number	Mean Temperature, ^{o}C	Standard Deviation
1. No preservative	20.62	0.17
2. NaOH	20.66	0.20
3. Na_2CO_3	20.58	0.14

Preservatives

Two preservatives were evaluated against the baseline case with no preservative added. They were sodium hydroxide and sodium carbonate. These solutions were prepared from reagent grade chemicals and MilliQ™ water. The initial quantities of the two solutions in the centrifuge tubes were 0.3 mL of 2.00 molar sodium hydroxide and 0.2 mL of 1.00 molar sodium carbonate solution.

Initiation of Experimental Runs

The equipment was assembled as described in Figure B-2. The pump was set to deliver ~1 mL min^{-1}. Two 3-way valves were used to direct flow to one train or the other or to bypass both trains. All lines were filled with air at the beginning of the experiment.

The feed sample line was purged to the feed sample collector through valve 1 and the desired flow rate achieved using unspiked feed solution. The purge solution was then replaced with ^{14}C spiked feed solution and the feed sample collection line purged for 5-12 min. An initial 1 mL feed solution sample was collected. The flow was redirected at valve 1 to fill the centrifuge tube in train 1. After filling the tube, valve 1 was switched and a second feed sample was collected. The flow was then redirected to fill the centrifuge tube in train 2 using valves 1 and 2. After filling the tube in train 2, valve 1 was again used to collect a third feed sample. The three samples of feed solution were used to determine the initial concentration of carbon-14 in the two centrifuge tubes.

Time was measured from the moment the first drop of sample entered the centrifuge tube. For sampling intervals in excess of 360 minutes, the apparatus was visited at least every 6 hours and the volume of impinger solution increased to a maximum of 13 mL with absolute ethanol to replace evaporation losses. The amount added was controlled so that at the end of the run the final volume was ~6 mL.

Sample Times

Continuous sampling was invoked. Absorbent solution was changed by replacing the midget impinger with another midget impinger containing fresh absorbent solution. The ^{14}C content was determined by transferring the absorbent solution to a liquid scintillation vial aided by two rinses (6 mL each) with liquid scintillation cocktail (Ecolume™), thus achieving nearly quantitative transfer of the sample to the vial. Each vial was counted for 100 minutes. Midget impingers were changed at 30, 125, 425, 1,374, and 4,374 minutes after initiation of each run. The rate of evaporation of ethanol in the

sampling solution and the degree to which it could be replenished during the interval limited the overall timing.

Quality Assurance

Since the objective was to determine relative losses (or ratios), ^{14}C standards were counted only at irregular intervals during the course of this work. When standards were processed, they fell within ±5% of the accepted value.

The performance of rotameters was confirmed by comparison of its rate to that computed for the travel of a soap bubble in a fixed volume bubble meter. The estimated uncertainty is ±1% at ambient temperature and pressure.

Results

The raw data are recorded in Table B-2. The pH of the solution in the fraction collector vials was not measured. A pH value for the vials was calculated based on the composition of the synthetic ground water and the amount and concentration of preservative in each vial using the computer program PHREEQC.

Table B-2. Net carbon-14 activity released from the fraction collector tube as a function of time.

Preservative		None Train 1	None Train 2	NaOH Train 1	NaOH Train 2	Na_2CO_3 Train 1	Na_2CO_3 Train 2
Elapsed Time (min)	Time Interval (min)	Impinger Activity (nCi)	Impinger Activity (nCi)	Impinger Activity (nCi)	Impinger Activity (nCi)	Impinger Activity (nCi)	Impinger Activity (nCi)
30	30	0.252	0.466	0.047	0.110	0.168	0.139
125	95	0.329	0.472	0.015	0.062	0.108	0.114
425	300	0.724	1.170	0.059	0.118	0.223	0.309
1,374	949	1.543	1.381	0.116	0.308	0.599	0.890
4,374	3000	0.806	1.391	0.130	0.116	0.424	0.325
Activity Lost		3.654	4.879	0.367	0.714	1.522	1.778
Initial Activity		60.122	60.122	48.922	48.922	47.349	47.286
	% Lost	6.08	8.12	0.75	1.46	3.21	3.76

Without a preservative, losses of $^{14}CO_2$ were about 7% over the three-day course of these experiments (Table B-3). Use of sodium carbonate as a preservative reduced $^{14}CO_2$ losses to 3½% over the same timeframe Addition of sodium hydroxide as a preservative instead of sodium carbonate reduced $^{14}CO_2$ losses to 1% over the same time frame. The retention of carbon-14 was highly correlated to the calculated pH of the solution in the centrifuge tube. Even with no preservative, carbon dioxide volatilization is less than 10% over three days.

Table B-3. Fraction of carbon-14 retained in the fraction collector tube as a function of time.

Preservative		None Train 1	None Train 2	NaOH Train 1	NaOH Train 2	Na_2CO_3 Train 1	Na_2CO_3 Train 2
Elapsed Time (min)	Time Interval (min)	Activity Retained (fraction)	Activity Retained (fraction)	Activity Retained (fraction)	Activity Retained (fraction)	Activity Retained (fraction)	Activity Retained (fraction)
30	30	0.996	0.992	0.999	0.998	0.996	0.997
125	95	0.990	0.984	0.999	0.996	0.994	0.995
425	300	0.978	0.965	0.997	0.994	0.989	0.988
1,374	949	0.953	0.942	0.995	0.988	0.977	0.969
4,374	3000	0.939	0.919	0.993	0.985	0.968	0.962

Conclusions

Use of sodium hydroxide or sodium carbonate solution as a preservative can reduce $^{14}CO_2$ losses from open tube collectors (Figure B-3). Sodium hydroxide provides better retention by creating a higher pH in the collection tube. Loss of carbon dioxide from collection tubes is at most a few percent over time periods of 8 to 12 hours, which is usually the maximum period between the time a fraction collector tube is filled and the tube is capped.

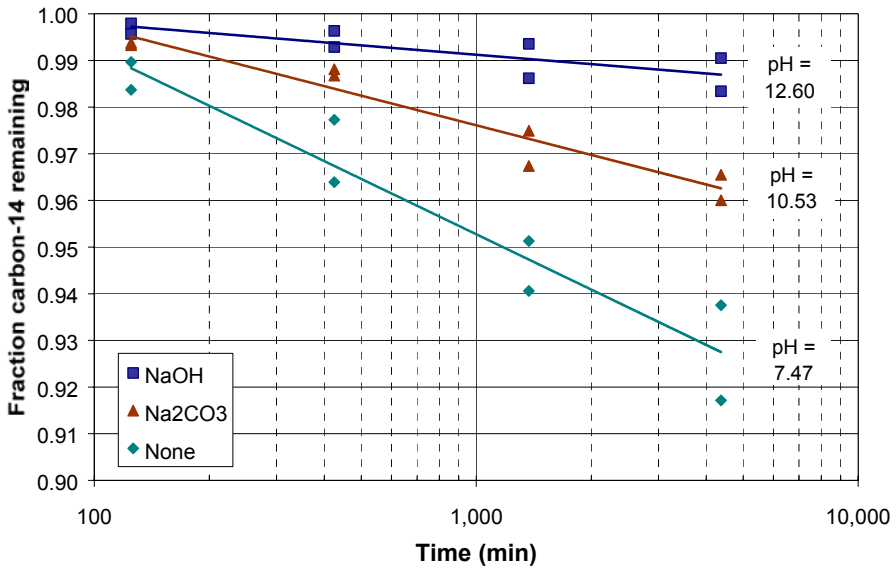

Figure B-3. Plot of the fraction of carbon-14 remaining in the fraction collector tube as a function of time for no preservative and two different preservatives. Retention is highly correlated to the pH of the solution in the fraction collector tube.

Appendix C

Description of the EFD1D Code for Estimation of Mass Flux from Gas Diffusion and Aqueous Advection in One-Dimension

Appendix C
Description of the EFD1D Code for Estimation of Mass Flux from Gas Diffusion and Aqueous Advection in One-Dimension

Arthur S. Rood

August 5, 1997

Revised September 28, 1998, January 9, 2001, March 6, 2001, June 7, 2001

The EFD1D (Explicit Finite Difference 1-Dimension) code was written to solve the problem of diffusive vapor phase transport and advective aqueous phase transport in a homogeneous isotropic media under flow conditions where the water content is assumed to remain constant. Partitioning between the vapor and aqueous phases is described by the dimensionless Henry's law constant. Partitioning between the aqueous and solid phases is described by the linear sorption coefficient. Boundary conditions include zero concentration at both ends of the model domain and an option for no-flux boundary on one end. In this revision to the model, a decay term has been added and temperature-dependent diffusion has been added.

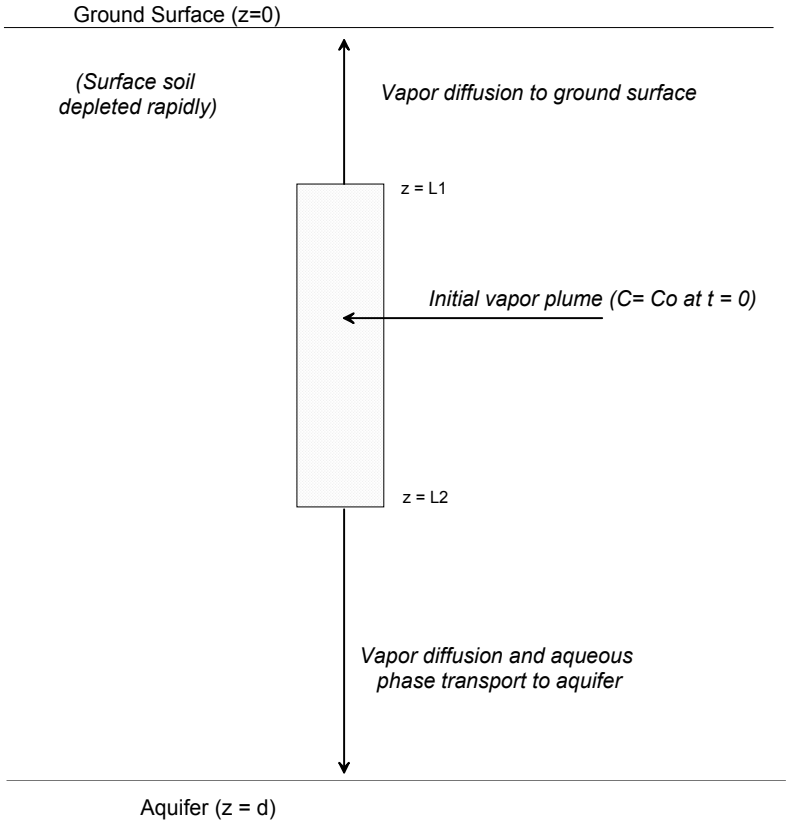

Figure C-1. Conceptual model of the EFD1D code for vapor diffusion and aqueous phase advective transport.

Consider the one-dimensional conceptual model illustrated in Figure C-1. An initial gas phase concentration is introduced into shaded area identified as the initial vapor plume. The top surface or boundary layer is assumed to be initially zero concentration. A fraction of the vapor partitions into the pore water and the remainder diffuses in the gas phase. The mass balance equation for one-dimensional gas and aqueous phase transport in the subsurface is

$$\frac{\partial\left(\phi_a C_a+\phi_g C_g+\phi_s C_s\right)}{\partial t}=\nabla\bullet\left(D_e\phi_g\nabla C_g-vC_a\right)+S-\lambda\left(\phi_a C_a+\phi_g C_g+\phi_s C_s\right) \tag{C-1}$$

where

C_a = the concentration in aqueous phase (M L^{-3})

C_g = the concentration in gas phase (M L^{-3})

C_s = the concentration in solid phase (M L^{-3})

ϕ_a = aqueous filled porosity

ϕ_g = gas filled porosity

ϕ_s = Fraction of media that is solid matrix or $1 - \phi_T$ where ϕ_T = total porosity

z = the depth below the surface (L)

v = the unsaturated Darcy velocity (L T^{-1})

D_e = the effective diffusion coefficient in the porous media (L^2 T^{-1})

S = a source in the gas phase (M L^{-3} T^{-1})

λ = decay rate constant (T^{-1})

The aqueous phase concentration is related to the gas concentration by the dimensionless Henry's law constant, H, and is given by $C_a = C_g/H$. The solid phase concentration is related to the aqueous phase concentration by the linear sorption coefficient or K_d, and is given by $C_s = K_d \rho_s C_a$. Equilibrium between the gas and aqueous phase is assumed. Equation (3) can be rewritten in terms of the gas phase concentration only, substituting the previously stated relationship for C_a and C_s. After some rearrangement it is given by

$$\frac{\partial C_g}{\partial t}=\nabla\bullet\left(\frac{D_e}{R_d}\nabla C_g-\frac{v}{H\phi_g R_d}C_g\right)+\frac{S}{R_d}-\lambda C_g \tag{C-2}$$

where R_d is given by

$$R_d=\frac{\phi_a}{H\phi_g}+1+\frac{K_d\rho_b}{\phi_g H},\quad \rho_b=\phi_s\rho_s \tag{C-3}$$

The direction of water flow is assumed to be downward into lower strata. Downward migration of the vapor is assumed to continue until a sink is encountered. The sink is represented by a zero concentration boundary condition and is applied at the last nodes in the model domain:

- $C_g = 0$, for $z = d$, for $t \geq 0$ (d = depth to aquifer)

For the top ($z = 0$), either a sink (zero concentration boundary condition) or a no-flux boundary condition can be applied

- $C_g = 0$, for $z = 0$, for $t \geq 0$ (d = depth to aquifer)

or

- $D_e \, dC_g/dz = 0$ at $z = 0$

Initial conditions are applied as follows

- $C = Co$ for $L_1 \leq z \leq L_2$ for $t = 0$ (see Figure 1)
- $C = 0$ for all other nodes

The effective diffusion coefficient in soil can be estimated by (Lyman et al. 1990)

$$D_e = D\left[\frac{\phi_g^{\,7/3}}{\phi_t^{\,2}}\right] \tag{C-4}$$

where

ϕ_t = the total effective porosity

D = the diffusion coefficient in air ($cm^2\ s^{-1}$).

The diffusion coefficient in air can be estimated by (Lyman et al. 1990)

$$D = \frac{10^{-3} T^{1.75} \sqrt{M_r}}{P\left(V_A^{1/3} + V_B^{1/3}\right)^2} \tag{C-5}$$

where

M_r = $(M_A + M_B)/(M_A M_B)$

M_A = molecular weight of air (28.97 g mol^{-1})

M_B = molecular weight of the contaminant

V_A = molar volume of air (20.1 cm^3 mol^{-1})

V_B = molar volume of contaminant

P = pressure (1 atm assumed)

T = temperature (K).

The temperature may vary as a function of depth below the surface and time of year. Assuming the soil has a constant thermal diffusivity and is infinitely deep, the temperature at depth z is given by

$$T(z,t)) = T_{avg} + A_o \exp\left(\frac{-z}{z_d}\right)\sin\left(\omega t - \frac{z}{z_d}\right) \quad \text{(C-6)}$$

where

z_d = damping depth $(2D_h/\omega)^{0.5}$

D_h = thermal diffusivity (0.051 cm^{-2} s^{-1})

ω = angular frequency (2π divided by the period [one year] s^{-1})

T_{avg} = annual average soil temperature (K)

A_o = amplitude of temperature change at soil surface (K)

In order to synchronize the time such that the simulation starts on January 1, a phase shift of 7π/2 is added within the sine term of equation 5.

The flux at any point in the model domain is given by Equation 7.

$$F = -\phi_g D_e \frac{\partial C_g}{\partial_z} + vC_g / H \quad \text{(C-7)}$$

Equation (2) was solved using an explicit finite difference technique described in Press et al. (1992). The cumulative flux was estimated by numerically integrating the flux from $t = 0$ to $t = t_e$, where t_e = the end time of the simulation. The ratio of the cumulative flux at the ground surface, to the total initial mass equals the fraction of contaminant released by upward diffusion. The initial mass (M) in the system is given by

$$M = A\int_0^d \phi_g C_{go}\ R_d\ dz \quad \text{(C-8)}$$

where

A = unit cross area (1 cm^2), d = length of the model domain

C_{go} = the initial gas phase concentration.

Time Steps and Grid Spacing

For simplicity, the code does not allow for variable grid spacing. Therefore, a single spacing distance is applied to all the nodes. The maximum number of nodes allowed is 1,200. The Peclet number should be evaluated when defining node spacing and, consequently, the number of nodes in a simulation. The Peclet number is given by

$$Pe = \frac{v\ \Delta x}{\phi_a\ D_e} \tag{C-9}$$

The Peclet number should be kept at a minimum, less than 1.0 and, preferably, less than 0.2. The Courant number is important in defining the time step used in the simulation and is given by

$$Cr = \frac{D_e\ \Delta t}{\Delta x^2} \tag{C-10}$$

for the diffusive component and

$$Cr = \frac{v\ \Delta t}{\phi_a\ \Delta x} \tag{C-ll}$$

for the advective component. The Courant number must not exceed unity for either the diffusive or advective component.

Finite Difference Solution

Equation (C-2) is solved using an explicit central finite difference approximation given by

$$\frac{C_g^{\,i+1,j} - C_g^{\,i,j}}{\Delta t} = \frac{\dfrac{\phi_g^{\,j-1} D_e^{\,i,j-1} C^{j-1}}{R_d^{\,j-1}} - \dfrac{2\phi_g^{\,j} D_e^{\,i,j} C^{j}}{R_d^{\,j}} + \dfrac{\phi_g^{\,j+1} D_e^{\,i,j+1} C^{j+1}}{R_d^{\,j+1}}}{\Delta x^2}$$
$$- \frac{v^{i+1} C_g^{\,j+1}}{\left(H\phi_g^{\,j+1} R_d^{\,j+1}\right)2\Delta x} - \frac{v^{i+1} C_g^{\,j-1}}{\left(H\phi_g^{\,j-1} R_d^{\,j-1}\right)2\Delta x} - \lambda C_g^{\,j} + \frac{S^{i,j}}{\phi_g^{\,j} R_d^{\,j}} \tag{C-12}$$

for $j = 2$ to n-1 where n = the number of finite difference nodes and i is the time index. Note that nodes 1 and n are boundary nodes. Boundary conditions include a zero concentration condition at either end of the model domain (*Dirichlet condition*), or a no-flux boundary condition at the surface ($x = 0$, *Neumann boundary*) and zero concentration at the aquifer [$C(n) = 0$]. The no-flux boundary condition is enforced by setting aside the first three nodes in the model domain (nodes 1, 2, and 3 from the surface). Node 1 is initially set at zero and node 3 is set equal to the value of node 1 [C(3)=C(1)] for each computational step. Mass in node 3 after each computational step is redistributed into node 4 in order to preserve mass balance.

Input to the code is through one ASCII file with the default file name of EFD1D.PAR. A line-by-line description of the input file is presented in Table C-1.

Table C-1. Input file format for the EFD1D code. Default file name is EFD1D.PAR. Comments can be added by placing a $ in the first column of a line.

Card Number	Variable	Code Variable	Type	Description
1		TITLE	CHARACTER	Title of problem solved
2		FILEOUT	CHARACTER	File name of output file
3		NN	INTEGER	Number of nodes
3		IBOUND	INTEGER	Flag for boundary conditions: (1) for zero concentration, (2) for no-flux (top of domain only)
3		ISRC	INTEGER	Flag for source type: (1) for no source updates, (2) for source updates
3		IVEL	INTEGER	Number of velocity vs. time points. If constant over time, enter 1 time-velocity point
3		ITEMP	INTEGER	Flag variable for temperature dependent diffusivity: 0 = no temperature dependence, 1 = temperature dependence.
NOTE: Card 4 is read only if ITEMP=1: All units must be input as specified. Calculations are performed in the same units				
4	*VA*	va	REAL	molar volume of air (20.1 cm^3 mol^{-1})
4	*VB*	vb	REAL	molar volume of contaminant (cm^3 mol^{-1})
4	*MA*	ma	REAL	molecular weight of air (28.97 g mol^{-1})
4	*MB*	mb	REAL	molecular weight of contaminant (g mol^{-1})
4	*P*	p	REAL	atmospheric pressure (atm)
4	T_{avg}	tavg	REAL	Average soil temperature (K)
4	*Ao*	a0	REAL	Amplitude of soil temperature at surface (K)
4	ω	omega	REAL	angular frequency (s–1)
4	D_h	dh	REAL	thermal diffusivity (cm^2 s^{-1})
4		phase	REAL	phase shift ($7\pi/2$ to start simulation at January 1st)
5	*D*	d	REAL	Free air diffusion coefficient (L^2 T^{-1})
5	*H*	H	REAL	Henry's law constant
5	λ	lambda	REAL	Decay constant (T^{-1})
5	K_d	kd	REAL	Sorption coefficient (L^3 M^{-1})
5	ρ_b	rho	REAL	Bulk density (M L^{-1})

Table C-1. (continued).

Card Number	Variable	Code Variable	Type	Description
5	--	a	REAL	Exponent in numerator of effective diffusion equation (7/3)
5	--	b	REAL	Exponent in denominator of effective diffusion coefficient (2)
NOTE: Card 6 is read IVEL times				
6	t	vt(i,1)	REAL	velocity vs. time - time
6	v	vt(i,2)	REAL	velocity vs. time - velocity (L T^{-1})
7		NL	INTEGER	number of points that describe air and water-filled porosity in model domain.
NOTE: Card 8 is read nl times. All nodes must be assigned an air and water-filled porosity				
8		n1	INTEGER	beginning node
8		n2		ending node
8	ϕ_g	PHIA	REAL	Air-filled porosity
8	ϕ_a	PHIW	REAL	Aqueous filled porosity
9	--	TEND	REAL	End time of simulation (T)
9	Δt	DT	REAL	Time step (T)
9	Δx	DX	REAL	Grid node spacing (L)
9	--	TSKIP	REAL	Number of time steps to skip between printing output
10	--	NNOUT	INTEGER	Number of output nodes (≤10)
10	--	NINI	INTEGER	Number of nodes to provide initial concentrations
11	--	NODEOUT(10)	INTEGER	Node number(s) to output (number of values must equal NNOUT)
NOTE: Card 12 is read NINI times. The default initial value is zero				
12	--	I	INTEGER	Node number
12	C_g	C	REAL	Initial gas phase concentration (M L^{-3})
NOTE: Cards 13 –15 are read only if ISRC=2.				
13	--	NSN	INTEGER	Number of nodes to provide source updates (maximum = 10)
14	--	ISN(10)	INTEGER	Node numbers for source updates
15	t	SRC(i,1)	REAL	Time for source update. A total of 500 time updates may be provided. The last time period must be ≥ TEND
15	S	SRC(i,j)	REAL	Source update for time i and node j (M/T) nodes read in order in which they are entered in variable ISN

Source Updates

Source updates are selected by setting the ISRC variable to 2. Source updates consist of a column of times (in the same units as the time step) followed by the total mass flux (e.g., g s^{-1}) of the tracer into the specified nodes in columns adjacent to the time column. The order of the source nodes is defined by the ISN variable which defines the source nodes. For example, if nodes 10,11, and 12 are defined as source nodes, then column 2 is the source for node 10, column 3 is the source for node 11 and so on. Column 1 is the time of source update. The last value of time must be greater than or equal to end time of the simulation (TEND). Note that in Equations (C-1) and (C-2) the source term has units of M L^{-3} T^{-1} (e.g., g m^{-3} s^{-1}) but the source updates are input in units of M T^{-1}. The source updates are converted to equivalent gas phase volumetric source units (M L^{-3} T^{-1}) in the code by the equation

$$S = \frac{Q}{A_u \Delta x} \tag{C-13}$$

where

Q = the mass flux into the source node (M T^{-1})

A_u = unit cross sectional area (L^2)

References

Lyman, W.J., W.F. Reehl, and D.H. Rosenblatt, 1990, *Handbook of Chemical Property Estimation Methods*. American Chemical Society, Washington DC.

Press, W.H., S.A. Teukolsky, W.T. Vetterling, and B.P. Flannery, 1992, *Numerical Recipes; The Art of Scientific Computing*. Cambridge University Press, New York.